Overproduction of hydrogen sulfide, generated by cystathionine β-synthase, disrupts brain wave patterns and contributes to neurobehavioral dysfunction in a rat model of down syndrome

Theodora Panagaki, Laura Lozano-Montes, Lucia Janickova, Karim Zuhra, Marcell Szabo, Tomas Majtan, Gregor Rainer, Damien Maréchal, Yann Herault, Csaba Szabo

Redox Biology 51 (2022) 102233

Contents lists available at ScienceDirect

Redox Biology

journal homepage: www.elsevier.com/locate/redox

Overproduction of hydrogen sulfide, generated by cystathionine β-synthase, disrupts brain wave patterns and contributes to neurobehavioral dysfunction in a rat model of down syndrome

Theodora Panagaki [a,1], Laura Lozano-Montes [a,b,1], Lucia Janickova [a], Karim Zuhra [a], Marcell P. Szabo [a], Tomas Majtan [a], Gregor Rainer [b], Damien Maréchal [c], Yann Herault [c], Csaba Szabo [a,*]

[a] Chair of Pharmacology, Faculty of Science and Medicine, University of Fribourg, Fribourg, Switzerland
[b] Visual Cognition Laboratory, Faculty of Science and Medicine, University of Fribourg, Fribourg, Switzerland
[c] Université de Strasbourg, CNRS, INSERM, Institut de Génétique et de Biologie Moléculaire et Cellulaire (IGBMC), Illkirch, France

ARTICLE INFO

Keywords:
Metabolism
Neurotoxicity
Gamma waves
Gasotransmitters
Trisomy

ABSTRACT

Using a novel rat model of Down syndrome (DS), the functional role of the cystathionine-β-synthase (CBS)/hydrogen sulfide (H_2S) pathway was investigated on the pathogenesis of brain wave pattern alterations and neurobehavioral dysfunction. Increased expression of CBS and subsequent overproduction of H_2S was observed in the brain of DS rats, with CBS primarily localizing to astrocytes and the vasculature. DS rats exhibited neurobehavioral defects, accompanied by a loss of gamma brain wave activity and a suppression of the expression of multiple pre- and postsynaptic proteins. Aminooxyacetate, a prototypical pharmacological inhibitor of CBS, increased the ability of the DS brain tissue to generate ATP *in vitro* and reversed the electrophysiological and neurobehavioral alterations *in vivo*. Thus, the CBS/H_2S pathway contributes to the pathogenesis of neurological dysfunction in DS, most likely through dysregulation of cellular bioenergetics and gene expression.

1. Introduction

Down syndrome (DS) – trisomy of all or part of human chromosome 21 (HSA21) – is the most common chromosomal disorder for intellectual disability [1,2]. A biochemical hallmark of DS is cellular bioenergetic dysfunction or pseudohypoxia [3,4]. Although there are more than 200 protein-coding genes on HSA21 that may contribute to this defect, recent evidence implicates a significant functional role of the genetic overdosage of cystathionine-β-synthase (CBS) [5–7]. According to this mechanism, the enzymatic product of CBS, the biological gaseous mediator hydrogen sulfide (H_2S) reversibly inhibits the mitochondrial Complex IV (cytochrome *c* oxidase) to induce mitochondrial dysfunction and a cellular bioenergetic defect [8]. Since this inhibition is biochemically reversible, pharmacological inhibition of CBS has the potential to improve bioenergetic (and, thereby, overall cellular functional) status, even in established DS. Indeed, in *in-vitro* studies, using various pharmacological CBS inhibitors, including the prototypical inhibitor aminooxyacetate (AOAA), were found to restore mitochondrial electron transport and ATP generation in human DS fibroblasts [8,9]. In an independent line of studies, CBS overexpression was shown to phenocopy the DS-like neurocognitive deficits in mice, while genetic deletion of CBS in DS mice has been shown to improve neurobehavioral function [10].

There are several rodent models of DS that carry partial or whole triplication of HSA21 or of orthologous genomic regions available. These models are characterized by various developmental and neurobehavioral defects and have been used for the last two decades to investigate the contribution of triplicated genes or groups of genes in the phenotype of DS, providing valuable insights into pathophysiological mechanisms and potential experimental therapeutic targets [11,12].

In the current study, we utilized a novel rat model that features a duplication of the segment of rat chromosome 20 (Rno20) consisting of 74 genes within the region *Umodl1* to *Prmt2* (Dup(Rno20)Yah) and includes the CBS gene [13]. We subchronically treated (Dup(Rno20)Yah) rats with AOAA (10 mg/kg per day) and assessed the efficacy of the

* Corresponding author. Chair of Pharmacology, Faculty of Science and Medicine, University of Fribourg, Chemin du Musée 18, Fribourg, 1700, Switzerland.
E-mail address: csaba.szabo@unifr.ch (C. Szabo).
[1] Equally contributed.

https://doi.org/10.1016/j.redox.2022.102233
Received 20 November 2021; Received in revised form 26 December 2021; Accepted 10 January 2022
Available online 13 January 2022

pharmacological inhibitor on animal spatial learning, spontaneous reference memory, social preference, and neural oscillation patterns. Our study provides *in-vivo* evidence for the functional role of the H_2S pathway on the alterations in brain metabolic and electrophysiological activity and cognitive function in Down syndrome.

2. Results

CBS is abundantly expressed in the DS brain and is localized in specific regions and cell types. A DS-associated increase in CBS expression was demonstrated using Western blots of homogenates of all four brain regions studied (Fig. 1A and B). In several DS brain regions, two CBS bands were detected, at the molecular weights consistent with the full-length 65 kDa and the 45 kDa proteolytically cleaved (but enzymatically active) [7] isoforms, respectively (Fig. 1A,C). The expression of the other two major enzymes associated with H_2S biogenesis showed variable effects. 3-MST expression was higher in DS compared to wild-type control brains in several regions studied, most prominently in the entorhinal cortex and the hippocampus (Fig. 1A,D). CSE expression was comparable in DS and healthy control rats in all brain regions studied (Fig. 1A,E).

With respect to the expression of the H_2S-degradation enzymes: TST expression was comparable in most DS and control brain regions, except for the entorhinal cortex where DS brains contained lower TST levels than controls (Fig. 2A,C). Similarly, the ETHE1 protein levels did not differ among the two studied genotypes in most brain regions studied, with the exception of the DS prefrontal cortex that exhibited slightly elevated levels (Fig. 2A and B). SQR protein expression was barely detectable in all of the brain regions studied and did not appear to be affected by DS or AOAA (Fig. 2D).

Interestingly, treatment of the rats with AOAA, a compound which is frequently used to inhibit CBS activity and H_2S biogenesis *in vivo* [7] had significant effect on the expression of several of the H_2S producing and degrading enzymes studied. AOAA normalized the truncated CBS levels in all DS brain regions assessed (Fig. 1A,C) and significantly decreased the overexpression of the full-length CBS in the DS hippocampus and entorhinal cortex (Fig. 1A and B). In the entorhinal cortex of DS rats, AOAA also attenuated the 3-MST overexpression (Fig. 1A,D). AOAA treatment also produced a suppression of the TST expression in several DS brain regions (Fig. 2).

Immunohistochemical analysis was used to identify the regions and cell types that predominantly express CBS in the DS brain. The most pronounced CBS expression was noted in astrocytes, but also vascular tissues surrounded by astrocytic end-feet exhibited CBS expression (Fig. 3). Prior studies have demonstrated increased expression of CBS in the brain of DS individuals; with high expression observed in astrocytes [14–17]. The current findings are consistent with these observations. The higher CBS expression in DS compared to wild-type controls, and

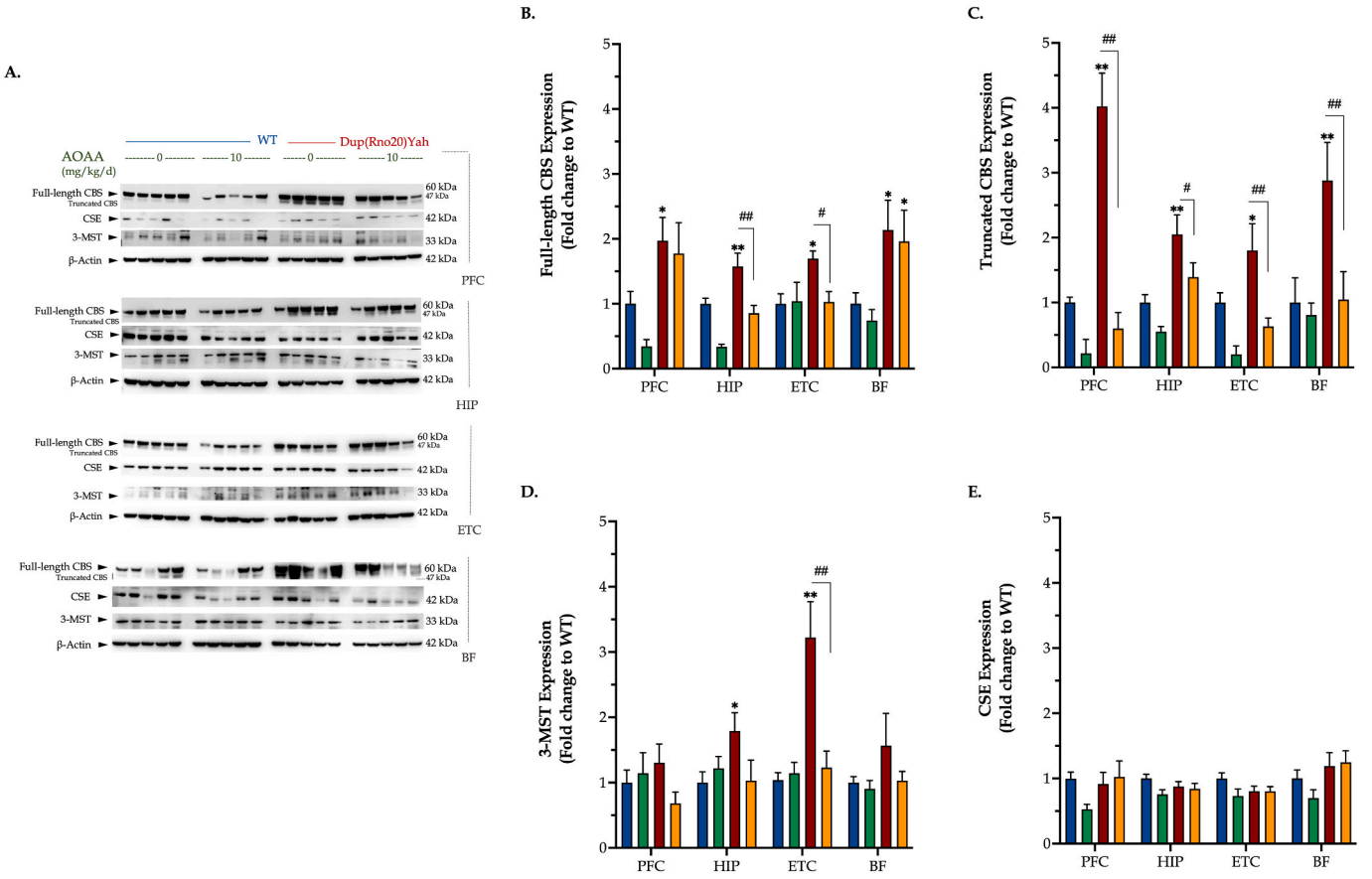

Fig. 1. DS is associated with the upregulation of CBS and 3-MST enzymes in a brain-region-specific manner. Following the cognitive assessment, animals were euthanized and tissue from the prefrontal cortex (PFC), hippocampus (HIP), entorhinal cortex (ETC), and the basal forebrain (BF) brain regions were collected for protein extraction. Protein samples were processed for immunoblotting detection of the H_2S producing enzymes cystathionine β-synthase (CBS) (A, B, C), 3-mercaptopyruvate sulfurtransferase (3MST) (A, D), and cystathionine γ-lyase (CSE) (A, E). (B): Quantification of the proteolytic, 45 kDa isoform of CBS. The expression of β-actin served as loading control for our analysis. Data, expressed as mean ± SEM of 5 animals per experimental condition, were analyzed by two-way ANOVA followed by *post hoc* Bonferroni multiple comparison *t*-tests at each brain region of interest. *$p \leq 0.05$ or **$p \leq 0.01$ shows significant differences between saline-treated DS rats and saline-treated WT rats; $^{\#}p \leq 0.05$ or $^{\#\#}p \leq 0.01$ shows significant effect of AOAA treatment on the expression of various H_2S-producing enzymes in Dup (Rno20)Yah rats.

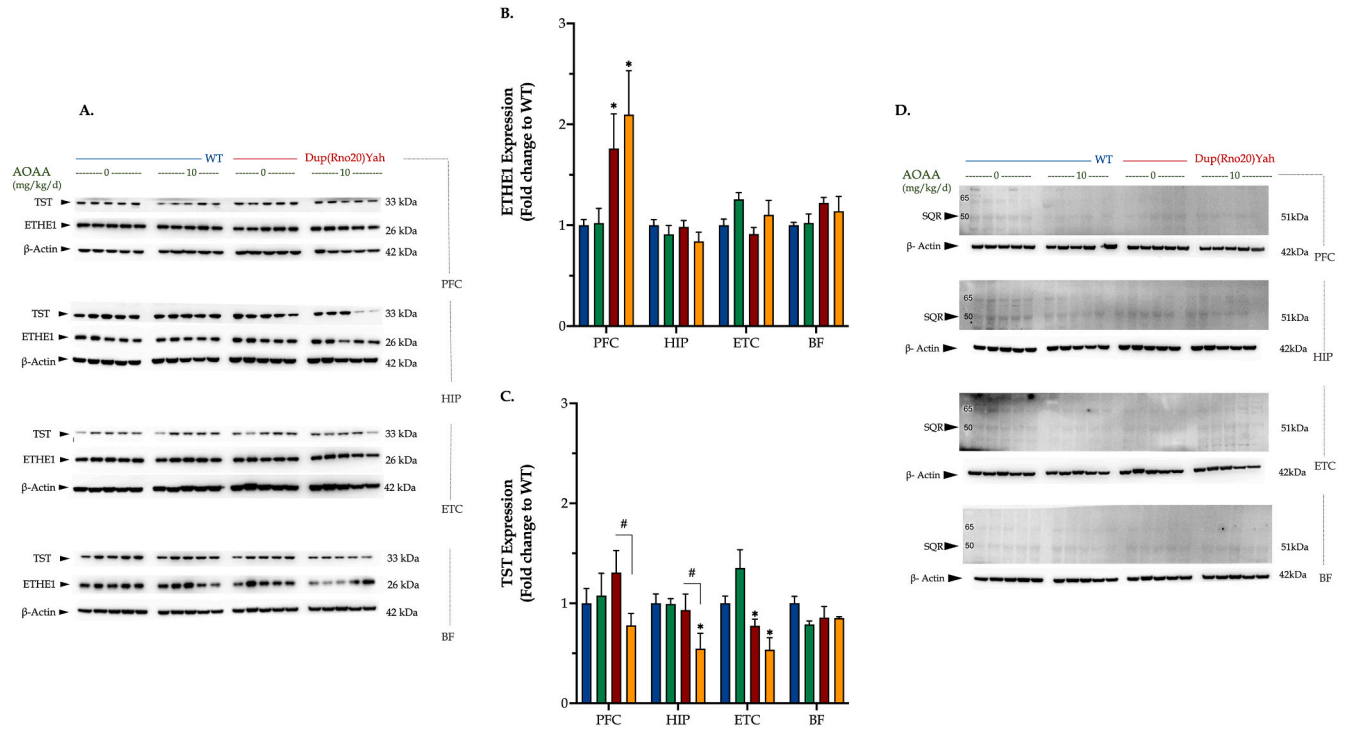

Fig. 2. DS differentially modulates the expression of various expression enzymes involved in H_2S degradation in a brain-region-specific manner. Following the cognitive assessment, animals were euthanized and tissue from the prefrontal cortex (PFC), hippocampus (HIP), entorhinal cortex (ETC), and the basal forebrain (BF) brain regions were collected for protein extraction. Protein samples were processed for immunoblotting detection of the H_2S catabolizing enzymes (A, B) ethylmalonic encephalopathy 1 protein (ETHE1), (A, C) rhodanese/thiosulfate sulfurtransferase (TST), and (D) sulfide quinone reductase (SQR). The expression of β-actin served as loading control for our analysis. Data, expressed as mean ± SEM of 5 animals per experimental condition, were analyzed by two-way ANOVA followed by *post hoc* Bonferroni multiple comparison *t*-tests at each brain region of interest. *$p \leq 0.05$ shows significant differences between saline-treated DS rats and saline-treated WT rats; $^{\#}p \leq 0.05$ shows significant effect of DS or AOAA treatment on the expression of various H_2S-regulating enzymes in Dup(Rno20)Yah rats.

the inhibitory effect of AOAA – effects already observed and quantified by Western blotting (Fig. 1) – was also confirmed by immunohistochemical analysis, as shown in a selected region (the C1 region of the hippocampus) in Fig. 4. Interestingly, the reactive astrogliosis a known feature of clinical DS [18] was also noted in our rat model and AOAA treatment reduced the number of astrocytes DS but not in control hippocampus (Fig. 4).

DS brain homogenates exhibit increased H_2S-producing activity, which modulates cellular bioenergetics. CBS enzymatic activity (assessed by the measurement of H_2S production in the presence of maximally stimulating substrate concentrations) was higher in all the tested DS brain regions than in corresponding control samples, with the entorhinal cortex (ETC) and the PFC showing the largest difference, and the basal forebrain (BF) and the hippocampus showing a smaller difference (Fig. 5). Addition of AOAA (100 μM) to the brain homogenates attenuated H_2S generation, suggesting that CBS is a significant source of H_2S generation both in the control and DS brains (Fig. 5). S-adenylmethionine (SAM), the physiological allosteric activator of CBS, stimulated H_2S generation in all brain regions studied, with a more pronounced effect in DS brains than in control brains (Fig. 5). Among the DS brain regions studied – in the presence of fully activated conditions, i.e. in the presence of SAM – the hippocampus showed the highest H_2S generation rates (approximately 2-times higher than in other regions), suggesting that this region may be a significant target for a cytotoxic effect of H_2S in DS.

Extracellular Flux Analysis, conducted in homogenates of hippocampal samples, indicated a trend for lower basal ATP generation in DS than in control brains; interestingly, *in vitro* treatment of hippocampal slices with AOAA increased ATP synthesis, without having an effect on ATP generation in the control group (Fig. 6). These findings can be interpreted as follows: there is a CBS/H_2S-mediated mitochondrial suppression in DS [6,8] – which, however, is compensated by the upregulation of other bioenergetic processes, e.g. an increase in aerobic glycolysis, as shown in multiple preclinical and clinical DS studies [3,4]. This compensatory increase in glycolytic ATP generation serves to maintain the tissue's baseline bioenergetic function. However, after CBS inhibition with AOAA, the reactivation of the mitochondrial electron transport chain produces an increase in ATP generation over baseline and control levels in the DS tissues (but does not have a significant effect in control tissues).

Subchronic CBS inhibition in control and DS rats is well tolerated and reveals a systemic metabolic dysfunction in DS. The CBS/H_2S pathway has been implicated in the regulation of a variety of physiological functions, including metabolism and gastric emptying [7]. In this light, we monitored the body weight of WT and DS rats weekly during the first two weeks of treatment. As shown in Fig. 7, no major effects of AOAA were noted. Hematological analysis with Vetscan® Whole Blood Analyzer revealed no significant differences in albumin, alkaline phosphatase, gamma-glutamyl transferase, globulin, calcium, magnesium, inorganic phosphorus, total protein, and urea nitrogen between control and DS rats or in the presence vs. absence of AOAA treatment; this finding indicates that (a) significant multi-organ dysfunction is not produced by this DS model and (b) AOAA does not adversely affect the function of major organs. However, interestingly, plasma levels of creatinine kinase (CK) were higher in the DS rats than in the control animals, and this was normalized by AOAA. Moreover, DS rats showed an elevation in aspartate aminotransferase (AST) plasma levels, indicative of a slight degree of hepatic dysfunction, which, once again, was normalized by AOAA (Fig. 7). Although the pharmacological effects of AOAA go beyond CBS inhibition (see further in the Discussion

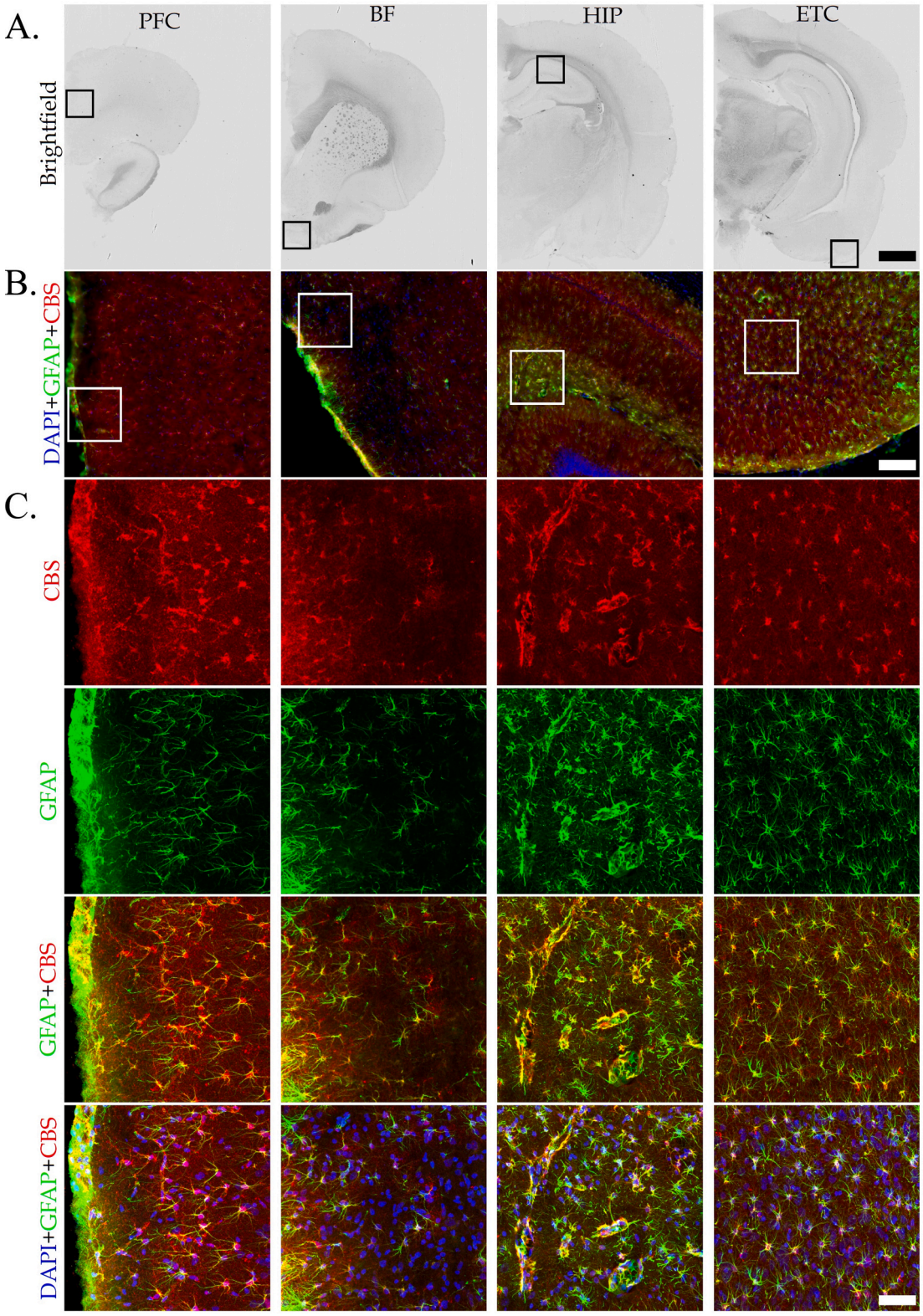

Fig. 3. CBS expression in the DS brain is localized in astrocytes and vascular tissues surrounded by astrocytic end-feet. Immunohistochemical staining of DS rat brain sections (40 μm thick) was analyzed in 4 different brain regions, including the prefrontal cortex (PFC), the basal forebrain (BF), the hippocampus (HIP), and the entorhinal cortex (ETC). Coronal brain sections were first scanned using the NanoZoomer in brightfield mode at small magnification in single layer (A). The regions of interest within different brain sections (black squares) were selected according to Paxinos-Franklin atlas and scanned using the NanoZoomer in fluorescent mode at 15X magnification (B), and confocal microscope at 40X magnification (C). Confocal images are shown as maximum intensity projection of the whole z-stack (40 μm), with z-step equal 0,42 μm. Scale bars represent 2 mm (A), 200 μm (B), and 60 μm (C), respectively. Immunofluorescence labeling for CBS (red), GFAP (green) and counterstaining with DAPI (blue) is shown. Identical acquisition settings were applied between different brain regions and groups. (For interpretation of the references to color in this figure legend, the reader is referred to the Web version of this article.)

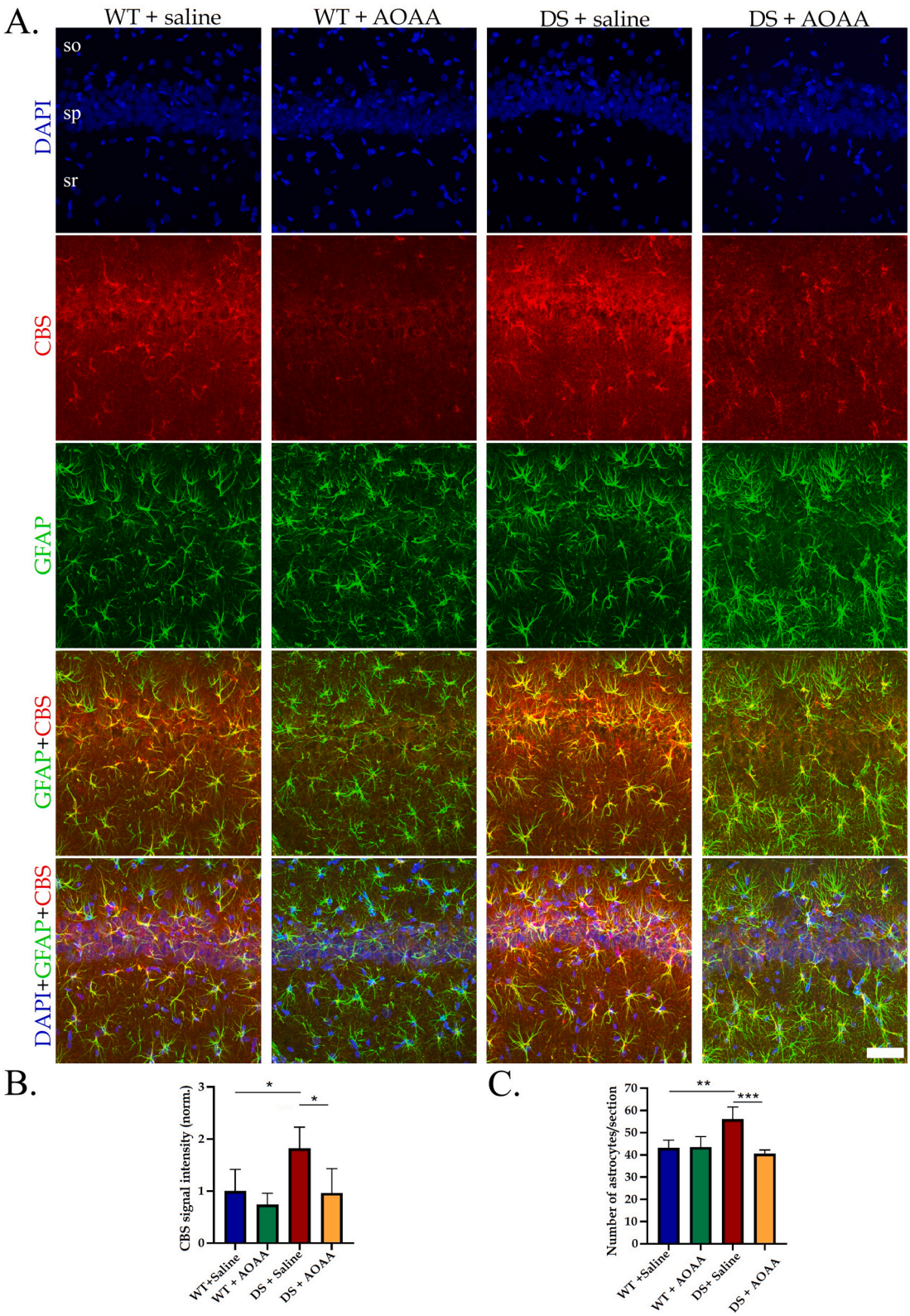

Fig. 4. AOAA treatment modulates CBS expression and reactive astrogliosis in the rat hippocampus in Down syndrome. (A): Immunohistochemical staining of CA1 region of rat hippocampus is shown, so: stratum oriens, sp: stratum pyramidale, sr: stratum radiatum. Coronal brain sections were scanned using the confocal microscope at 40 x magnification using the same acquisition settings between different groups. Immunofluorescence labeling for DAPI (blue), CBS (red), and GFAP (green) is shown. Scale bar represents 60 μm. Quantification of CBS signal intensity (B) and number of astrocytes per section (C) was done using the Imaris software. Data are expressed as mean ± SD of 4–5 animals per experimental condition. Data were analyzed by two-way ANOVA followed Tukey multiple comparison test, *$p \leq 0.05$; **$p \leq 0.01$; ***$p \leq 0.001$. (For interpretation of the references to color in this figure legend, the reader is referred to the Web version of this article.)

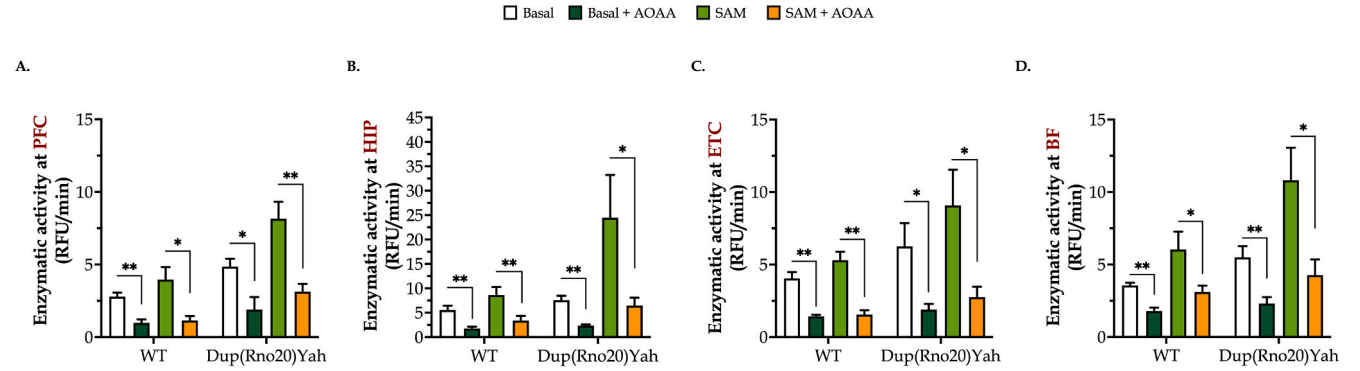

Fig. 5. DS brain tissues produce more H_2S than control tissues in a region-specific manner. Brains from control or Dup(Rno20)Yah rats were dissected into coronal sections of 1 mm, and the regions of (A) the prefrontal cortex (PFC), (B) hippocampus (HIP), (C) entorhinal cortex (ETC), and (D) basal forebrain (BF) were isolated. They were treated with 0 or 100 μM AOAA for 1h at 37 °C and homogenized. Samples were followingly incubated with cysteine and homocysteine in the presence or absence of the allosteric CBS activator S-adenosylmethionine (SAM). Maximally stimulated enzymatic H_2S generation, which estimates the maximal capacity of the tissue to produce H_2S (rather than basal levels of H_2S in the absence of exogenous substrates, which produce low and barely detectable levels in this assay) was measured by following the increase of fluorescence of the AzMC probe over time. Data, expressed as mean ± SEM of 6 animals per experimental condition, were analyzed by two-way ANOVA followed by *post hoc* Bonferroni multiple comparison *t*-tests. *p ≤ 0.05 and **p ≤ 0.01 indicate the inhibitory effect AOAA on H_2S generation.

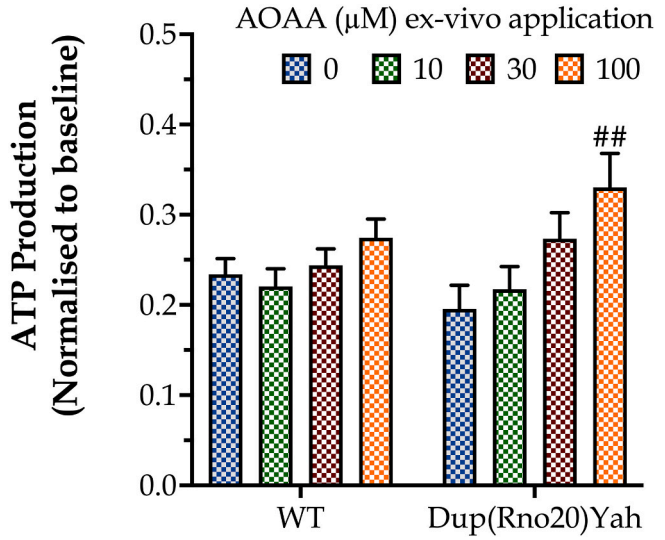

Fig. 6. The CBS inhibitor AOAA selectively increases ATP generation in DS hippocampal tissue. Hippocampal tissues from control or Dup(Rno20)Yah rats were obtained with punch biopsies and subjected to Extracellular Flux Analysis after incubation were treated with 0 or 100 μM AOAA for 1h at 37 °C. Data, expressed as mean ± SEM of 6 animals per experimental condition, were analyzed by two-way ANOVA followed by *post hoc* Bonferroni multiple comparison *t*-tests. ##p ≤ 0.01 shows the stimulatory effect of 100 μM AOAA on ATP generation in the Dup(Rno20)Yah group.

section), one possible interpretation of the findings is the following: the slightly elevated CK and AST levels may indicate a modest degree of cardiac, skeletal muscle and/or hepatic dysfunction in DS which may be, at least in part, due to H_2S-related cytotoxic or metabolic suppressive effects.

The CBS/H_2S pathway is not involved in the regulation of spatial working memory in the rat. In the T-maze paradigm, DS animals and control animals displayed comparable latency times until their first entry to the goal arm of the maze, with a mean of 12 successful entries and a success rate of 60% within the first minute of the retention trial. Two weeks of AOAA treatment did not significantly affect the T-maze responses (Fig. 8). These findings suggest that the CBS/H_2S pathway does not regulate spatial working memory formation in control rats or in DS.

The CBS/H_2S pathway contributes to the spontaneous place recognition memory defects associated with DS. Next, we evaluated spatial components of the episodic memory in the object location paradigm. A familiarization session with the open-field arena preceded the task acquisition, during which animal locomotor activity and anxiety levels were assessed. As shown by the tracking paths, animals featured comparable ambulatory activity in the arena; control rats in vehicle-control group (saline), control rats subjected to AOAA treatment, DS rats treated with vehicle, and DS rats in AOAA covered a total length of 26.3±1.1, 25.2±2.3, 30.2±1.8 and 24.9±1.6 m, respectively, which was similarly traveled per minute among the groups over the 10-min session (Fig. 9). We also quantified the animals' activity in the center and the corners of the arena to determine any emotional defects that may have impacted the acquisition of the object location task. As shown in Fig. 9, control and DS rats explored the center for 36±7 s and 27±4 s, respectively, in ~17 and 15 total entries in the area of interest over the 10-min session. These findings indicate similar anxiety levels between the two groups of animals that were additionally kept low, evidenced by the low percentages of thigmotaxis per minute of arena exploration. AOAA treatment had no significant effect on the aforementioned parameters. Importantly, however, DS rats failed to recall the familiar object location, as compared to their controls, scoring below chance levels in the retention trial (Fig. 10). These memory defects did not result from impaired task acquisition; WT and DS rats featured similar exploration times during the sample session. AOAA treatment restored the DS-related suppressed Recognition Index for the novel location to control levels, without significantly affecting the performance of the control animals.

Pharmacological inhibition of CBS rescues DS-associated defects in social recognition memory in the rat model. Some people with DS display autism spectrum disorders [19]. Thus we tested here if the DS rat model Dup(RNO20) is associated with an abnormal social behavior and if the treatment can change this behavior. We used a classical social test and we found that the DS rats exhibit impaired animal sociability, with the DS rats devoting similar exploring times between the object and the male conspecific available in the arena over the task acquisition trial. Thus, the behavior of DS rats contrasts the phenotype of the control rats, which spend 2/3 of their total exploration time interacting with the available social target (Fig. 11). These behavioral defects of the DS model correlate well with a significantly suppressed discrimination between the novel and familiar conspecifics compared to controls, scoring below the chance level in the retention

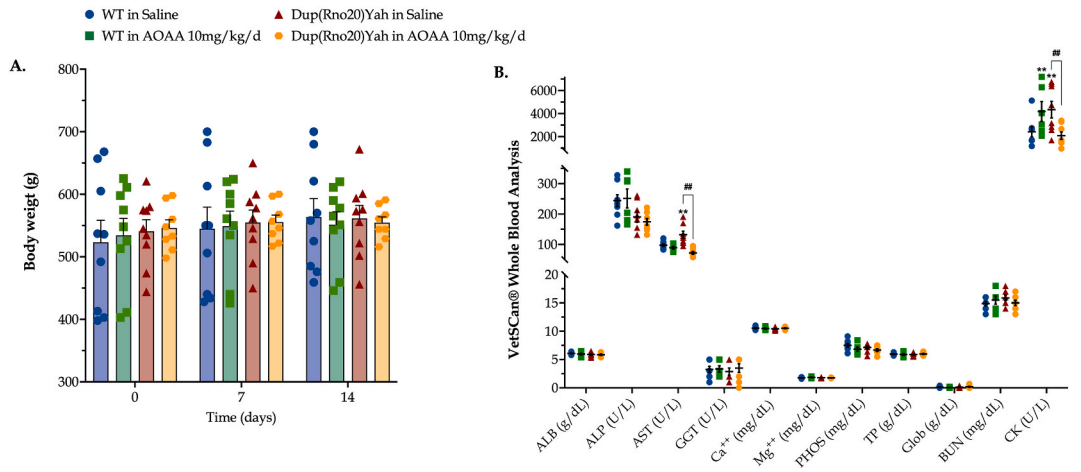

Fig. 7. Effect of the CBS inhibitor on AOAA on body weight and systemic markers or organ function in control and DS rats. (A): Body weight of the rats, monitored weekly for two weeks following the initiation of the intraperitoneal administration of saline or AOAA (10 mg/kg/d). (B): At the end of the study, upon animal euthanasia, trunk blood was collected and processed with VetScan® Analyzer for analysis of circulating markers of organ function. Each dot represents one animal per experimental condition. The mean ± SEM per experimental condition was additionally calculated and plotted as bar graphs and lines in subfigures (A) and (B), respectively. Weight data (n =11 per experimental group) were analyzed by two-way ANOVA at each time point and hematological data (n=8 per experimental group) were processed with three-way ANOVA analysis followed by *post-hoc* analysis with Bonferroni correction. **p≤0.01 shows significant differences between saline-treated DS rats and saline-treated WT rats; $^{\#\#}p \leq 0.01$ shows significant effect of AOAA treatment in Dup(Rno20)Yah rats, indicative of improved organ function.

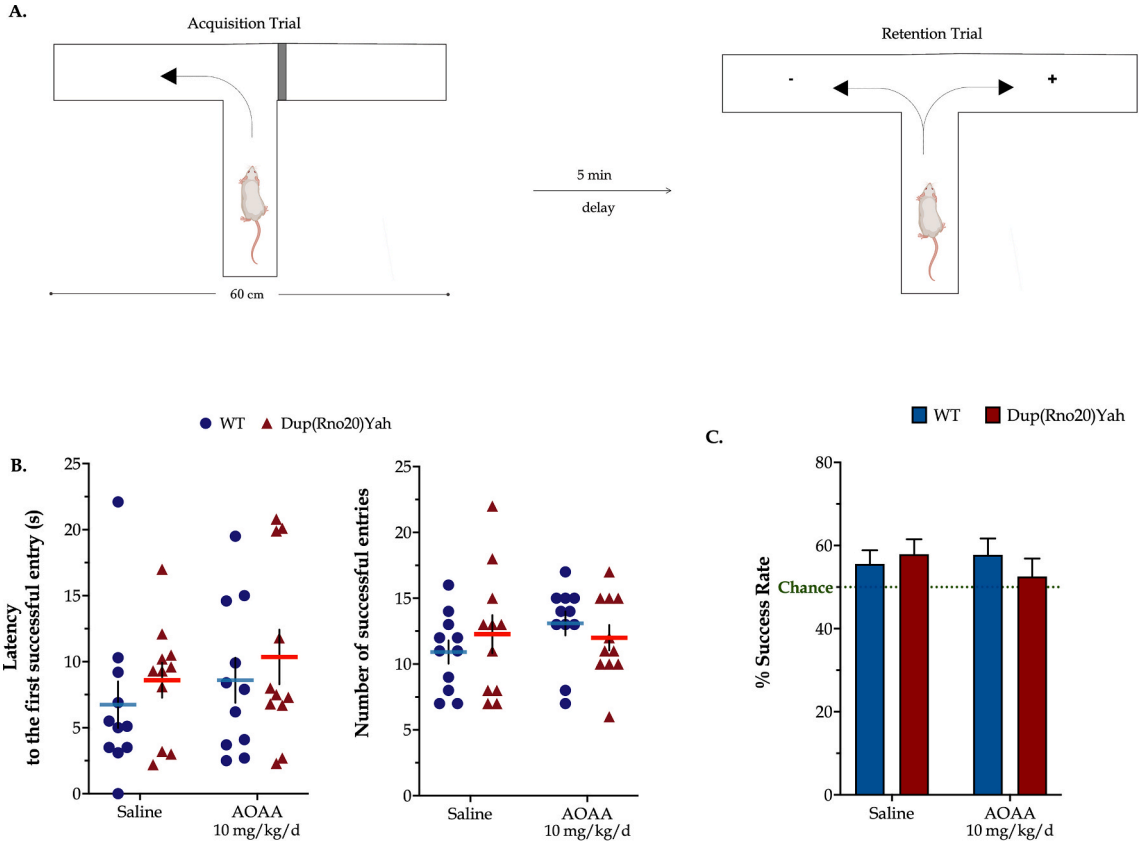

Fig. 8. Neither the genetic overdosage of CBS nor the pharmacological inhibition of CBS enzyme activity affects spontaneous alteration *in vivo*. (A): Schematic representation of the forced T-maze task. During the acquisition trial, the tested rats were forced to select and explore the left arm of the apparatus. After a 5-min delay, each testing subject was placed into the starting arm and allowed to explore the maze with both left and right arms accessible. Every entry of the rat to the unfamiliar, right arm of the apparatus (annotated with the "+" symbol) represented a spontaneous alteration event and counted as a success. (B): The latency till the first successful entry along with the number of successful entries to the novel arm during the retention trial was monitored. (C): *Success Rate* was further calculated based on the allotted time to the novel arm over the total time in both arms engaged by each testing subject. Each dot plot represents one animal. *Success Rate* data were expressed as mean ± SEM of 11 rats per experimental condition and plotted as bar graphs. No significant differences were noted between any of the experimental groups studied.

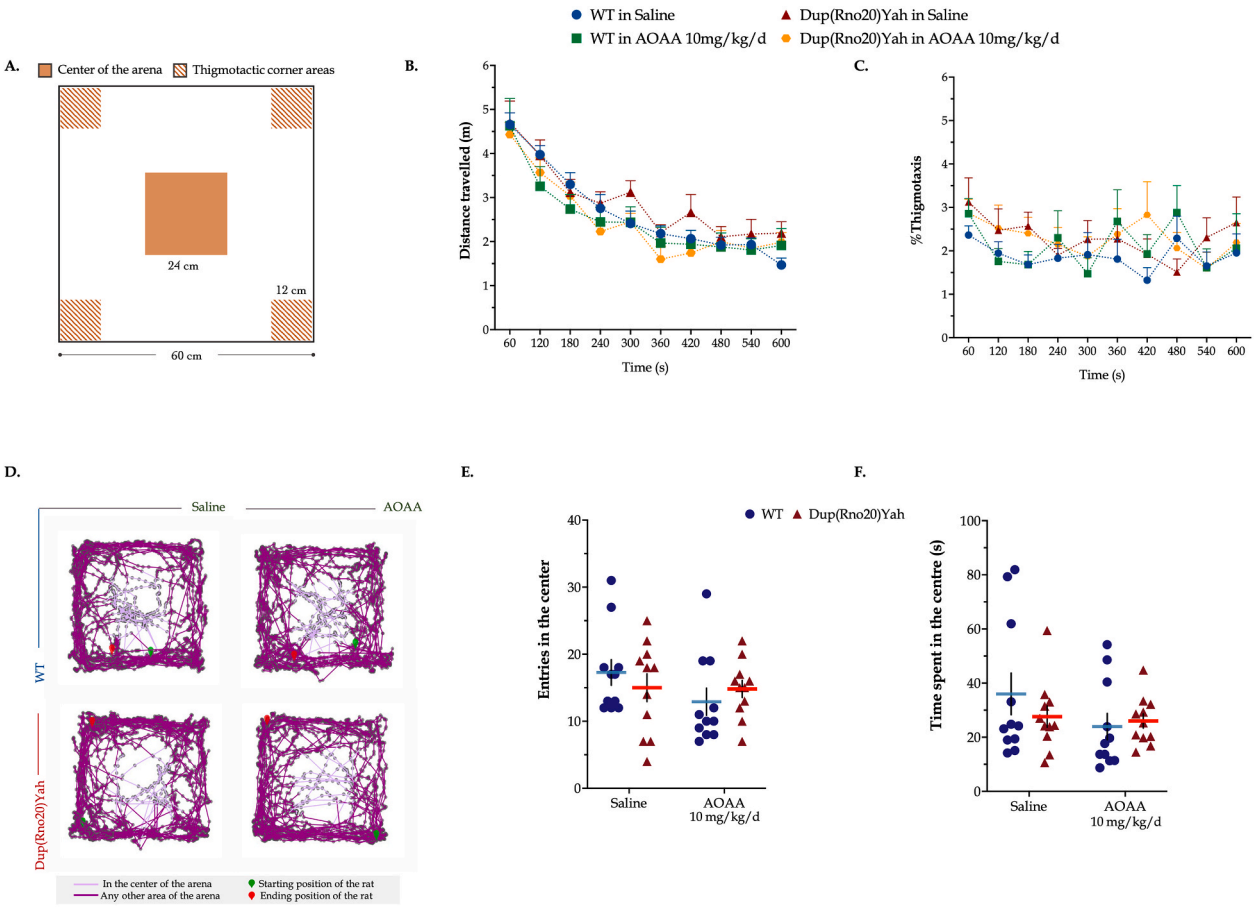

Fig. 9. Dup(Rno20)Yah rats exhibit normal locomotion and exploratory behavior. (A): Schematic representation of the open field arena annotated with the areas of interest used for assessing the emotional status and exploratory/risk-taking behaviors. (B): The total distance traveled along with (C): % thigmotaxis – which defines the percentage of time allotted in hanging in corner areas – per minute was monitor over the 10-min arena familiarization session. (D): Representative tracking maps annotated with all acquired positions of the animal in the arena in dark purple and the path followed in the center in light purple. (E): The total number along with the (F) total time spent in the center of the arena were monitored to evaluate exploratory/risk-taking behavior in this animal-aversed zone. Each dot plot represents one animal. Each symbol represents the mean ± SEM of 11 rats per experimental condition. No significant differences were noted between any of the experimental groups studied. (For interpretation of the references to color in this figure legend, the reader is referred to the Web version of this article.)

trial. CBS inhibition significantly rescued the DS-related impairment in social recognition memory and rendered it back to control levels, although the AOAA-treated DS rats performed similarly to the corresponding saline-treated ones during the task acquisition (Fig. 11). Importantly, pharmacological inhibition of CBS did not exert any negative effect on the behavior and memory of control rats.

The CBS/H_2S pathway regulates synaptic protein expression and brain electrical activity in DS. Increasing evidence attributes the disrupted cognitive function in DS to underlying synaptopathy that mainly involves dendritic dysgenesis, diminished synapse formation, and immature dendritic spine [20]. We quantified the expression levels of the presynaptic vesicle protein, synaptophysin – and the scaffolding protein for dendritic spine dynamics – PSD95 in key brain regions for attention, navigation, and memory [20]. DS hippocampus, ETC, and basal forebrain exhibited a significantly decreased expression of PSD95, that was restored by *in vivo* CBS inhibition (Fig. 12). In addition, hippocampal synaptophysin was significantly suppressed in DS when compared to control, and CBS inhibition also rescued this impaired expression and further promoted the expression of synaptophysin across the prefrontal and entorhinal cortex of the DS rat brain (Fig. 12).

Consistently with the biochemical synaptic data, the brain electrical activity within the ETC and basal forebrain of the DS rat model exhibited significant spectral alterations in the DS rats, with a significant decrease in γ oscillations. AOAA treatment restored γ activity and further stimulates θ and β oscillations of the DS basal forebrain area (Fig. 13).

3. Discussion

Due to a "gene dosage effect", the elevation of CBS mRNA and CBS protein in individuals with DS has been well established for several decades [14–17]. Pierre Kamoun and his colleagues have demonstrated that DS individuals exhibit increased urinary levels of the stable H_2S metabolite thiosulfate [21,22], a finding that has been also confirmed by an independent group [23]. According to the "Kamoun Hypothesis" [5], the excess H_2S exerts cytostatic and/or cytotoxic effects in DS, due to its metabolic inhibitory effect, thereby identifying CBS as a potential therapeutic target. Work conducted in recent years has confirmed and expanded on this hypothesis, and has demonstrated that in DS fibroblasts there is a metabolic inhibition (suppression of mitochondrial electron transport and aerobic ATP generation, driven primarily by a reversible suppression of mitochondrial electron transport chain complex IV by H_2S) [8]. Meta-analysis of DS studies conducted over the last two decades suggests that this suppression of aerobic ATP generation is, at least in part, compensated by an upregulation of aerobic glycolysis, which "makes up" for part of ATP generation, but also produces excess lactate, which can be readily detected in the plasma of DS individuals [3,4]. Our working hypothesis [6] is that this bioenergetic imbalance makes DS individuals viable, but the energetic defects may manifest, for

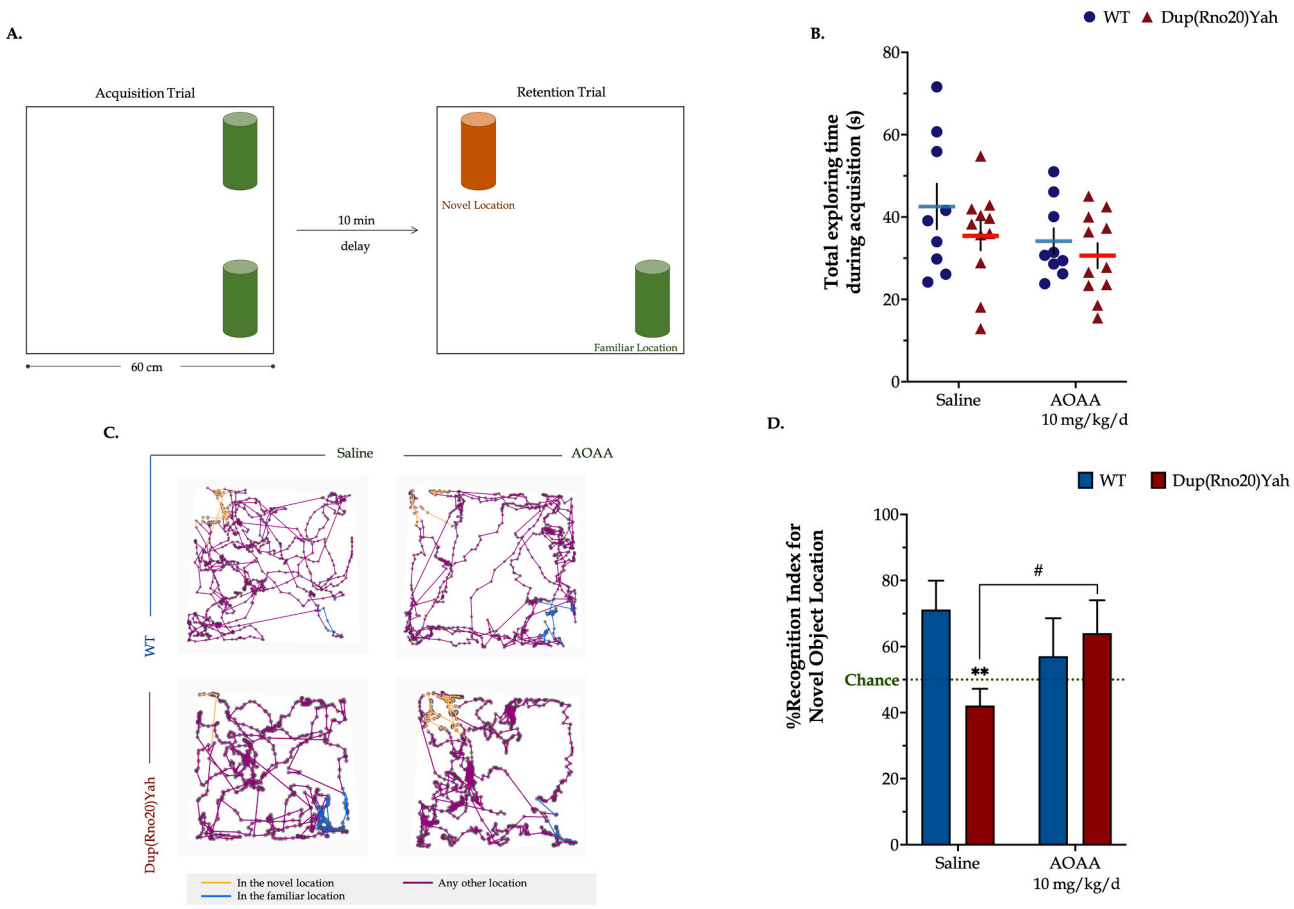

Fig. 10. Dup(Rno20)Yah rats exhibit suppressed recognition memory that is restored by CBS inhibition. (A): Schematic representation of the object-location recognition paradigm. (B): The time allotted in exploring the objects available in the apparatus during the 5-min acquisition trial. (C): Representative tracking maps that are annotated with all acquired positions of the animal in the arena in dark purple along with the path followed in the novel and familiar locations in light orange and blue colors, respectively. (D): The Recognition Index for the novel object location, calculated as the percent ratio of the time spent in the novel location of the object over the total exploration time and assessed during the retention trial. Each dot plot represents one animal. Each bar represents the mean ± SEM of 11 independent rats per experimental condition. Data were analyzed with two-way ANOVA analysis followed by *post hoc* Bonferroni's multiple comparison *t*-tests. **$p \leq 0.01$ shows significant differences between saline-treated DS rats and saline-treated WT rats; $^{\#}p \leq 0.05$ shows significant effect of AOAA treatment in Dup(Rno20)Yah rats, indicative of restoration of recognition memory of these animals. (For interpretation of the references to color in this figure legend, the reader is referred to the Web version of this article.)

instance, in reduced exercise tolerance, as well as – potentially – in altered neurological and/or muscle function [4,6]. Recent *in vivo* studies have, in fact, indicated that forced overexpression of CBS in the mouse brain, on its own, can produce neurobehavioral defects associated with DS, and preliminary pharmacological studies with disulfiram, a multifunctional compound – which, among other pharmacological effects, acts as a CBS inhibitor *in vivo* [9,10] –, improves neurological function in a mouse model of DS [10].

The genes that are triplicated in human DS, in mice, are distributed onto three different chromosomes [11]. Importantly, many of the DS models used in the literature contain triplications of many genes but not CBS, and therefore are not directly comparable to the results of the prior DS/CBS study [10] or the current rat study, where CBS triplication is incorporated into the experimental model. The above findings also suggest that (a) DS-like neurobehavioral phenotypes can be induced by triplicating genes other than cbs, and (b) the CBS-associated metabolic and functional defects in human DS develop on the background of multiple other defects. Indeed, DS is not only associated with dysregulation of genes and corresponding proteins encoded on Chromosome 21 (or its murine equivalents), but also with dysregulation of genes encoded on other chromosomes [4]. The above caveats notwithstanding, the results of the current study, which utilized a commonly used CBS inhibitor, AOAA [24,25], indicate that H_2S may significantly contribute to some of the metabolic and neurocognitive, as well as electrophysiological alterations associated with DS. These data also indicate that the CBS/H_2S-associated impairments in DS can be pharmacologically reversible over the course of a relative short time; in the current study, a 2-week treatment with AOAA was sufficient to improve several functional parameters, including (a) bioenergetic parameters, (b) neurobehavioral parameters, (c) reactive astrogliosis, (d) dysregulated expression of various synaptic proteins, (e) brain electrophysiological activity and even (f) several plasma markers of organ impairment in the periphery. Although, clearly, DS is associated with numerous developmental/anatomical defects, which may not be readily reversible, it appears that some of the DS-associated functional impairments (including neurobehavioral and learning dysfunction) can be pharmacologically reversible over a relatively short treatment duration.

The generation of H_2S in mammalian cells and tissues is a dynamic process, regulated by several enzymes. H_2S biogenesis is primarily catalyzed by CBS, CSE and 3-MST. Our results presented in Figs. 1–4 suggest that CBS, and/or its product, H_2S, may cross-regulate the expression of several enzymes involved in the regulation of H_2S homeostasis in the brain. First of all, although not encoded on Chromosome 21, studies in DS fibroblasts have recently indicated that DS is

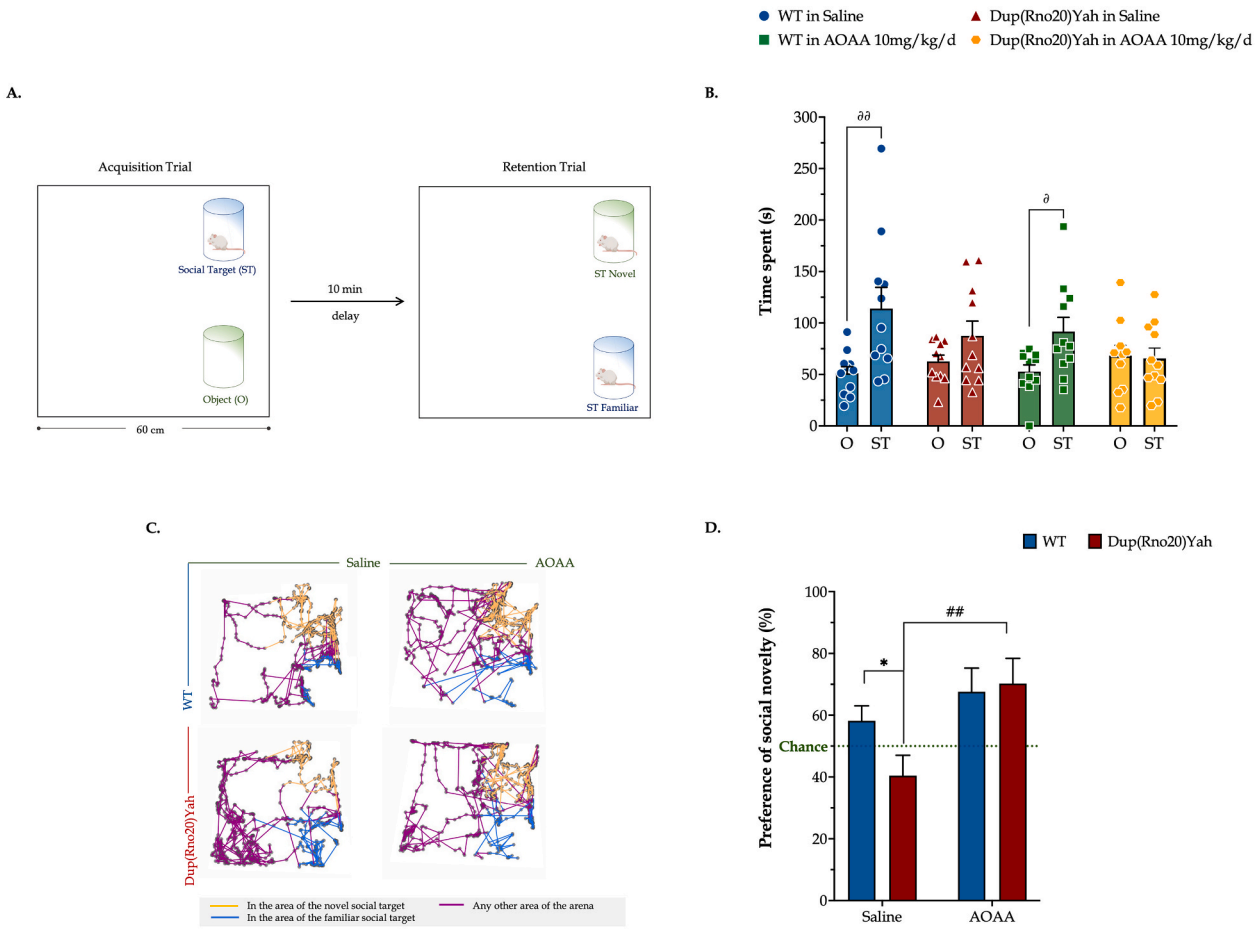

Fig. 11. Dup(Rno20)Yah rats exhibit an impaired preference for social novelty that is normalized by CBS inhibition. (A): Schematic representation of the setup of the social preference paradigm. During acquisition, the arena was enriched with two identical transparent cylindrical cages for sociability; one cage contained a male conspecific, and the second one remained empty. (B): The time spent exploring either target during the 5-min acquisition trial was recorded and plotted herein. After 10 min, rats underwent a retention trial during which the previously encountered juvenile rat was placed in the previously empty cage and a second juvenile male rat – unfamiliar with the test subject – was added to the cylindrical cage that was previously occupied. The activity of the tested subjects in the arena was tracked for another 5 min. (C): Representative tracking maps that are annotated with the general path traveled and colored in dark purple along with the locations acquired for interacting with the novel and familiar conspecific in light orange and blue colors, respectively. (D) Preference Index for the novel social target ("Preference of social novelty"), calculated as the percent ratio of the time interacting with the novel conspecific over the total time allotted in social interaction during the retention trial. Each dot plot represents one animal. Each bar represents the mean ± SEM of 11 rats per experimental condition. Data acquired during acquisition and retention trials were, respectively, analyzed with a three-way and two-way ANOVA analysis followed by post hoc Bonferroni's multiple comparison *t*-test. *$p \leq 0.05$ shows significant differences between O and ST responses in WT rats; $^{\partial}p \leq 0.05$ or $^{\partial\partial}p \leq 0.01$ shows significant differences in the time allotted to the object exploration within control rats (either saline-treated or AOAA-treated); $^{\#\#}p \leq 0.01$ shows significant effect of AOAA in Dup(Rno20)Yah, indicating normalization of the animals' social novelty preference. (For interpretation of the references to color in this figure legend, the reader is referred to the Web version of this article.)

associated with an upregulation of 3-MST [26], and this upregulation was also evident in the current study in various brain regions of DS rats. 3-MST which may be a secondary source of excess H_2S or polysulfides in DS, and its functional role *in vivo* remains to be subject to future investigations. Importantly, H_2S levels are determined not only by production, but also by degradation. This is driven by several enzymes, including rhodanese and ETHE1 and SQR. ETHE1, in our experimental model, was affected (upregulated) in DS in some brain regions (e.g. the prefrontal cortex), perhaps as a compensatory mechanism to facilitate the degradation of the excess H_2S in DS. As previously noted for the CNS [27], the expression of SQR was very low in all brain regions studied and did not appear to be affected by DS or AOAA.

There is currently insufficient information regarding the potential brain-region-specific differences in the regulation or action of various CBS or H_2S related pathways; thus, it is difficult to formulate a mechanistic hypothesis as to why certain changes in the expression of some of the above enzymes are unique to certain brain regions, but not others. For instance, it may be logical to hypothesize that the upregulation of TST in the prefrontal cortex may be a compensatory reaction to the elevated CBS and 3-MST (and, consequently, H_2S and polysulfide) levels, but this hypothesis would not explain why a similar upregulation did not occur in the entorhinal cortex, where DS was associated with a similar upregulation of CBS and 3-MST. The molecular mechanisms underlying the variable and brain-region-specific effects of AOAA on the expression of CBS, 3-MST, TST and ETHE-1 remain to be further investigated as well. In this context, the observations that (1) various H_2S producing enzymes can cross-regulate each other, (2) that AOAA can, indeed, suppress the expression of CBS or 3-MST, and (3) that H_2S donation can increase CBS, TST or SQR expression has already been observed in various cell types and experimental models *in vitro* and *in vivo* [28–31]. Potential feedback mechanisms involving the regulation of H_2S of the mRNA expression and/or degradation of these enzymes have been hypothesized, but the underlying molecular mechanisms remain to be further investigated.

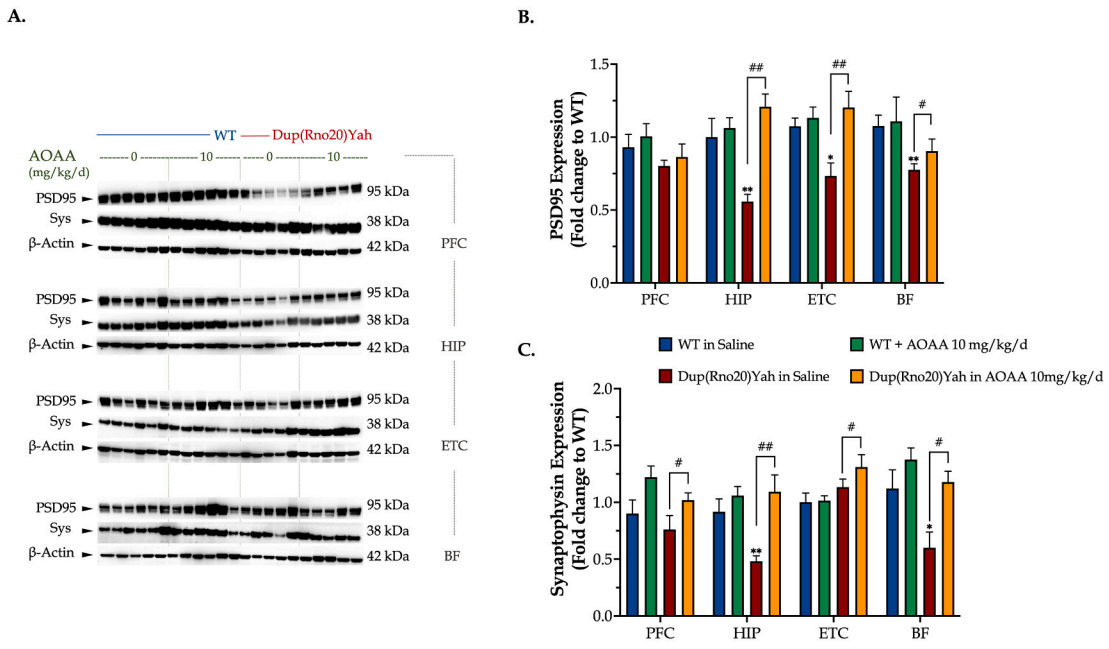

Fig. 12. DS impairs synaptic protein expression in the brain; restoration by CBS inhibition. Following the cognitive assessment, animals were euthanized and tissue from the prefrontal cortex (PFC), hippocampus (HIP), entorhinal cortex (ETC), and the basal forebrain (BF) brain regions were collected for protein extraction. Protein samples were processed for immunoblotting detection of (A, B) the post-synaptic density protein 95 (PSD95) and (A, C) synaptophysin (Sys). The expression β-actin served as a loading control. Data were expressed as mean ± SEM of 6 animals per experimental condition, except for saline-treated DS where data were expressed as mean ± SEM of 5 animals. Data were analyzed by two-way ANOVA followed by *post hoc* Bonferroni multiple comparison *t*-tests at each brain region of interest. *p≤0.05 or **p≤0.01 shows significant differences between saline-treated DS rats and saline-treated WT rats; $^{\#}$p≤0.05 or $^{\#\#}$p≤0.01 shows significant effect of AOAA treatment in Dup(Rno20)Yah rats, indicative of restoration of synaptic protein expression.

In the context of the role of alterations in H_2S degradation in the pathogenesis of CNS injury, it is interesting to mention the neurological disease ETHE1 deficiency, where H_2S degradation is impaired, which, in turn, produces elevated (and neurotoxic) H_2S levels, and corresponding adverse effects, most likely via metabolic/bioenergetic inhibition [32]. We must emphasize that physiological levels of H_2S have drastically different roles than the pathologically elevated levels associated with DS and ETHE1 deficiency. Under physiological conditions, H_2S has neuromodulatory and neuroprotective roles, and inhibition of these roles may exert adverse effects, perhaps after long-term and complete inhibition of H_2S biosynthesis. Thus, the likely "best" CBS-inhibition-based therapeutic approach in DS would be the one where H_2S *overproduction* is normalized (i.e. reduced to healthy control levels), but the enzyme is not completely inhibited. This approach would also be expected to reduce the risk of the side effect of CBS inhibition, i.e. homocysteinemia, since one of the physiological roles of CBS (primarily, hepatic CBS) is in the process of transsulfuration, where it contributes to the metabolism and elimination of circulating homocysteine [7,33].

The changes in brain wave spectra in the DS rats shown in the current study are interesting, and so is the fact that these spectral changes could be restored by pharmacological CBS inhibitors. Indeed, γ oscillations have received significant attention over recent years; these spectral activities are, at least in part, generated or modulated by AMPA and GABA receptor activity. These oscillations are associated with the "quiet wakefulness" state (sometimes characterized as an "introspective state") of the animals [34]. The current findings are in line with results of an electrophysiological study utilizing the transgenic DS model TgDyrk1A, where γ oscillations have been found to be reduced, perhaps in the context of a reduction in recurrent inhibition as a mechanism that may contribute to DS-associated cognitive deficits [35]. There are several reports demonstrating a variety of brain waves in DS individuals [36]. Another study, using a different DS model, also reported significant alterations of γ-oscillations and hypothesized that these changes could play a role in the pathophysiology of well-documented sleep disruptions in DS children [37]. It is also interesting, in the context of longer-term neuropathological alterations associated with DS (see below) that γ oscillations are known to be impaired in Alzheimer's disease (AD): this impairment correlates with the increased amyloid load in the CNS [38]. In fact, pharmacological restoration of γ oscillations is now considered a potential therapeutic approach to counteract various neurodegenerative processes [39].

The results presented in the current study demonstrate that CBS inhibition affects the expression of various proteins either associated with the modulation of H_2S homeostasis, and/or with the modulation of various synaptic functions. DS is associated with a significant degree of dysregulation of various genes, both encoded on Chromosome 21 and on other chromosomes [4,40,41]. The mechanisms how CBS and/or H_2S affects gene expression are currently unknown. Nevertheless, there are several prior examples demonstrating that H_2S can affect the expression or binding of various transcription factors, and can affect the expression of many mRNAs and the proteins encoded by them [42–47].

Are there specific cell types and anatomical regions, then, that are primarily affected by the CBS/H_2S pathomechanism? Clearly, the current experiments and prior studies in human DS clinical materials [16,17] both indicate the involvement of astrocytes, as one of the tissue types where CBS is most predominantly expressed. Indeed, the pathophysiological role of astrocytes in DS has previously been suggested several independent studies [48–52]. In this context it is interesting that AOAA treatment of the animals reduced the astrocytosis that was observed in the DS hippocampus (Fig. 4C). Indeed, astroglial cells are known to respond to trauma and ischemia with reactive gliosis, a reaction characterized by increased astrocytic proliferation and hypertrophy. A common feature and pathological hallmark of several CNS diseases is reactive astrogliosis [18,48–52]. Astrogliosis is a dynamic process, which is modulated by hormones or various pharmacological agents, and it has been considered a potential target for experimental therapy [53]. It is possible that higher intracellular H_2S levels in DS astrocytes are directly driving astrocyte proliferation, but it is also

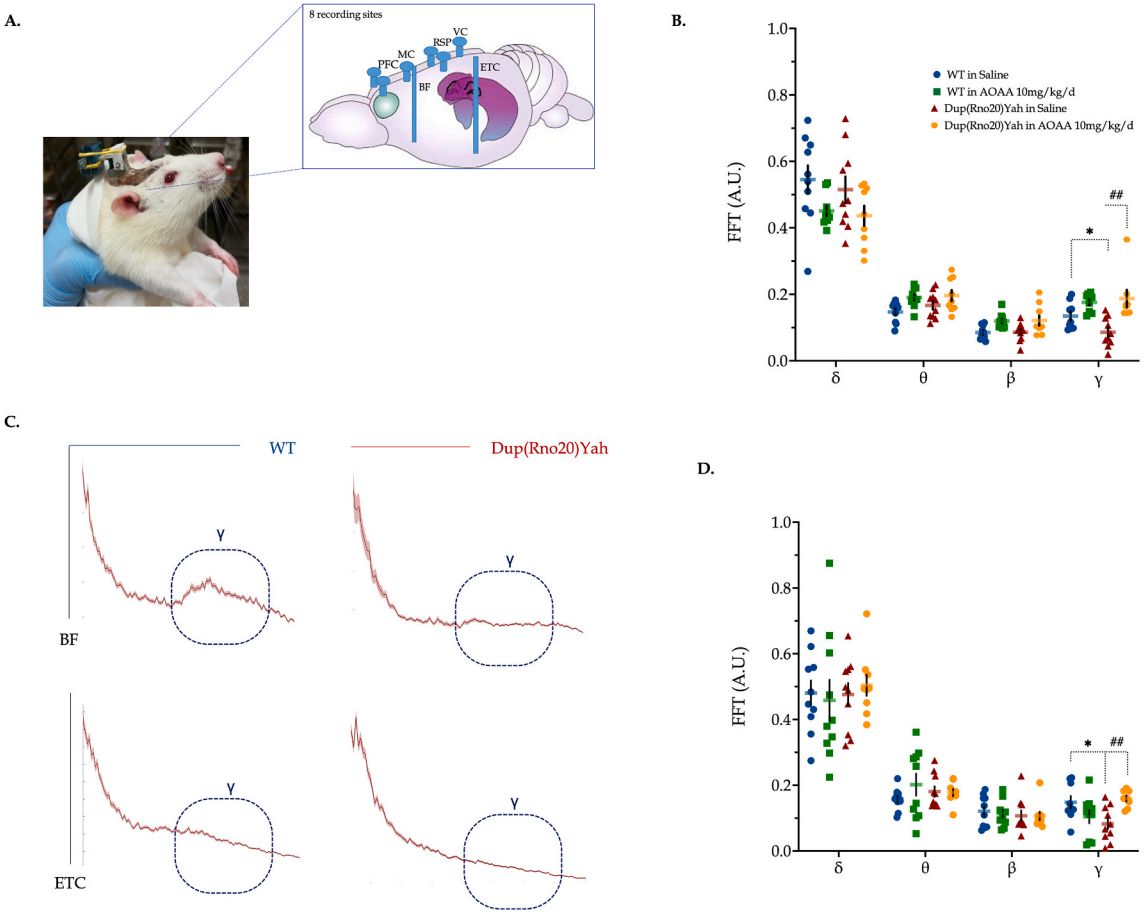

Fig. 13. DS **impairs electrical wave patterns in the rat brain; restoration by CBS inhibition. (A)** Representative image for the connectors on the head of rats, along with the differential position of microelectrodes across the brain. Recordings of the brain activity were taken from freely moving animals during behavioral testing in the open field arena. Power spectra were calculated for each epoch by fast Fourier transform; γ activity was calculated by taking the mean value of the power spectrum between 30 and 80 Hz in (B) basal forebrain (BF) and (D) entorhinal cortex (ETC). (C): Representative spectra highlighted with the γ oscillations from the BF and ETC regions of WT and Dup(Rno20)Yah rats. Each point represents one animal. Data were analyzed by two-way ANOVA followed by *post hoc* Bonferroni multiple comparison t-tests at each brain region of interest. *$p \leq 0.05$ shows significant differences between saline-treated DS rats and saline-treated WT rats; $^{\#\#}p \leq 0.01$ shows significant effect of AOAA treatment in Dup(Rno20)Yah rats, indicative of normalization of brain wave patterns.

possible that after inhibition of CBS, the overall improvement in CNS function and homeostasis in the DS brain indirectly reduces the number of astrocytes. The underlying mechanisms of AOAA's action on astrocyte numbers remain to be further investigated.

The expression of CBS in vascular tissues may also suggest a more general (diffuse) H_2S-related pathomechanism in multiple parts of the brain. Of importance, the significant amount of blood vessels in the brain are surrounded by astrocytic end-feet and hence could represent key mediators for the cognitive deficits induced by neurovascular dysfunction. Naturally, H_2S, as a diffusible mediator, can readily exit one cell type (where it is produced) and affect surrounding cell types or even may have access to remote tissues via the circulation.

Measurements of *ex vivo* H_2S generation performed in the current study suggest that the hippocampus may be one of the most significant sources (and possible target) H_2S overproduction. Indeed, the hippocampus is one of the brain regions with the highest relative percentage of astrocytes [51] and a significant brain region involved in learning and memory deficits in DS [51–54]. Other neuroanatomical systems including prefrontal cortex are also relevant to cognitive functions and could influence attention, memory and cognitive flexibility. Moreover, there is a considerable amount of literature reporting on specific projections between basal forebrain and its cortical targets, or between hippocampus and entorhinal cortex that modulate cognitive functions and play important role for episodic memory and temporal associative learning [55].

As mentioned earlier, some DS individuals display autism spectrum disorders [18]. Indeed, the current experimental model Dup(RNO20) appears to produce abnormal social behavior and, as such, may be considered a mixed experimental model, rather than a "DS model". The effect of AOAA on social recognition impairments was prominent in the current study. Social behavioral defects are not generally considered characteristic features of DS but rather are typical features in patients on the autistic spectrum (and such alterations can also be seen in various murine models of autism) [56–58]. Indeed, there are a wide range of DS rodent models, which – depending on the particular type of chromosome triplication and associated gene expression effects and compensatory effects – produce a variety of neurobehavioral responses [11–13], some of which may be characteristic for autistic behavior. Although the mechanistic connection between DS and autism has not yet been sufficiently explored, some common pathways (e.g. DYRK1) have been recently identified, and certain pharmacological agents (e.g. a pharmacological inhibitor of the Na^+-K^+-Cl-importer) appears to show efficacy both in autism and DS models [59–62]. Further work is required to explore the potential connection of DS and autism and the potential involvement of various H_2S-associated pathways.

In the early childhood and young adulthood, the progressive learning disability represents the biggest challenge in DS. In adulthood, Alzheimer-like neuropathological symptoms develop as well. In fact, the

current classifications consider DS a genetic form of AD, where all of the neuropathological features (i.e. plaque formation) as well as the functional consequences are predominantly represented [63]. The molecular pathogenesis of DS-associated AD is poorly understood. Based on the emerging role of the CBS/H_2S pathway in DS, and the associated bioenergetic linkage discussed above, we hypothesize that DS-associated AD may also have a CBS/H_2S related component, perhaps, once again, linked to bioenergetic process. The processing and elimination of amyloid precursor proteins is, indeed, an energetically demanding process: bioenergetic blockade can lead to improper processing/elimination of these proteins, and, consequently, plaque accumulation and neurotoxicity [64]. Recent studies demonstrate that oxidative phosphorylation is markedly dysregulated in the brain in a mouse model of DS and AD [65]. Indeed, mitochondrial bioenergetic dysfunction and associated defects in protein processing have been already implicated in many forms of neurodegeneration [66–72]. In this context, it is interesting to note that Kanaumi and colleagues have previously detected a marked increase in CBS-positive astrocytes around senile plaques in adults with DS [17]. Future experiments (for instance, via utilization of the current model of DS) will be needed to directly test contribution of the CBS pathway to the pathogenesis of AD-like neuropathologies in DS.

Many of the conclusions of the current study are based on the effects of AOAA. This agent, although used in hundreds of prior *in vivo* studies to inhibit CBS [reviewed in 7] and is commonly referred to as a "CBS inhibitor" should be considered with caution. First of all, *in vitro* studies in human recombinant CBS and CSE enzyme have demonstrated that AOAA is a comparable inhibitor of both [24]. Although the effect of AOAA on H_2S generation from CSE vs. CBS in cell-based systems has not yet been comprehensively investigated, we can assume that the effects of AOAA reported in various *in vitro* and *in vivo* models may be the product of a combined inhibition of both of these H_2S-producing enzymes. The fact that AOAA inhibits both CBS and CSE follows from its mode of action, which involves a direct interaction with the PLP prosthetic group in the active center of these enzymes [7]. However, AOAA should not be viewed as an indiscriminate inhibitor of *all* PLP-dependent enzymes, in fact, most PLP-dependent enzymes investigated so far are *not* inhibited by this compound [7,73]. However, it does inhibit several members of the PLP-dependent enzyme class, including GABA-transaminase [7, 74–83]. Thus, the mechanism of AOAA's action in the current study may include, in addition to CBS inhibition, CSE inhibition, as well as GABA-T inhibition. The latter effect would be expected to increase GABA levels in the CNS; in fact, AOAA < at the dose levels used in the current study has previously been shown to elevate GABA levels in various brain regions [7,74–83]. Nevertheless, the majority of the DS literature does not implicate GABA deficiency as a significant pathogenetic factor in DS; in fact, the evidence points toward a GABA-mediated overinhibition, and the therapeutic effects of GABA receptor blockers [84–86]. In this context, a GABA-T inhibition-induced elevation of CNS GABA levels by AOAA would not be consistent with improved neurocognition in DS. On the other hand, stimulation of GABA pathways has been linked to benefit in autism models [87,88]; thus, an AOAA-mediated elevation of CNS GABA levels would be, in fact, consistent with an improved performance in autistic-related defects studied in the current project, e.g. the social recognition assay.

We would like to emphasize that the beneficial neurobehavioral effects in murine DS models have previously been reported with genetic normalization of CBS, as well as effects with disulfiram (which has CBS inhibitory effects *in vivo,* although it also has additional pharmacological actions as well) [9,10]. Thus, based on the results of the current study – taken together with multiple independent studies implicating the CBS/H_2S pathway in the pathogenesis of DS [3–6] – indicate that H_2S overproduction is a likely pathogenetic factor in DS and CBS inhibition should be considered as a potential future experimental therapeutic target to improve the neurocognitive function associated with DS. Nevertheless, the possibility remains that additional molecular targets (CSE, GABA-T and possible additional targets) may also have contributed to some of the functional and/or bioenergetic effects of AOAA demonstrated in the current study. Clearly, a selective and potent CBS inhibitor is needed to further extend the current findings – as well as to serve as a potential prototype for the future experimental therapy of DS. Currently no clinically applicable CBS inhibitors exist, although there are several multifunctional and potentially repurposable clinically approved drugs (e.g. disulfiram and benserazide) which have CBS inhibitory (as well as several additional) pharmacological effects [7,9, 10,73]. Further work on the molecular pathogenesis of this pathway in DS, coupled with the identification of novel, potent and selective CBS inhibitors may lead to the experimental therapeutic exploitation of CBS as an emerging therapeutic target in DS.

4. Methods

Animals. In the rat (*Rattus norvegicus*) genome, the Hsa21 homologous regions are located on two chromosomes, Rno11 and Rno20. On Rno11, the Lipi-Zbtb21 segment is almost identical to the homologous region located on the Mmu16, whereas Rno20 harbors a unique segment for the Umodl1-Prmt2 interval. The Rno20 region contains the rat cbs gene. The transgenic Sprague-Dawley Dup(Rno20)Yah rat model of DS, containing the duplication of Rno20 [13] was developed at the Institute of Genetics and Molecular and Cellular Biology (IGBMC, Illkirch-Graffenstaden, France). Wild-type (WT) female rats of the same background were acquired from Janvier Labs (Le Genest-Saint-Isle, France). Following acclimatization for a week, the WT female rats were paired with the heterozygous Dup(Rno20)Yah males in the vivarium of the University of Fribourg. Their offspring were ear-punched and genotyped by polymerase chain reaction with sequence-specific primers (PCR-SSP) (Table 1). Male offspring negative for the targeted mutation served as the healthy control group, while their male littermates carrying the duplication formed the DS experimental groups. Rats were housed in a temperature-controlled colony room (21 ± 2 °C), in conventional cages enriched with fine Aspen bedding, standard nesting material, and standard fun tunnel of carton paper. Animals were under a 12h light/dark cycle, and *ad-libitum* access to food and water.

Daily handling of the animals for a week preceded the surgical implantation of optic fibers and electrodes, as described in the following subsection. Following a two-week recovery from the surgery, animals were randomly assigned to control and experimental treatments that referred to the administration of saline (0.9% Sodium Chloride) and 10 mg/kg AOAA (CAS No: 2921-14-4, Sigma-Aldrich Chemie GmbH, Buchs, Switzerland), respectively. Both treatments were dosed at a volume of 1 ml, once a daily via the intraperitoneal (IP) route for a total of 18 days. During the last 8 days of the administration, the exploratory behavior and cognitive functioning of the rats were assessed in the tasks of the forced alternation T-maze, open field, object location recognition, and social preference. A day-off in between the different behavioral tasks was incorporated into the protocol. Animals were additionally monitored for their body weight once per week over the treatment period. All experimental procedures and animal handling carried out during the light phase, with at least an hour gap from the light/dark

Table 1
Primers used for animal genotyping.

Duplication	9371	GGTCTCATCGTGGCCCATACTC	MUTANT FORWARD
	9373	CAAGCACACAAGTCGTTGCTGAG	MUTANT REVERSE
Wild-type allele specific for 3′-part of the targeted locus	9371	GGTCTCATCGTGGCCCATACTC	INTERNAL POSITIVE CONTROL FORWARD
	9372	GTTCATCTTGGAACCCGGTG	INTERNAL POSITIVE CONTROL REVERSE

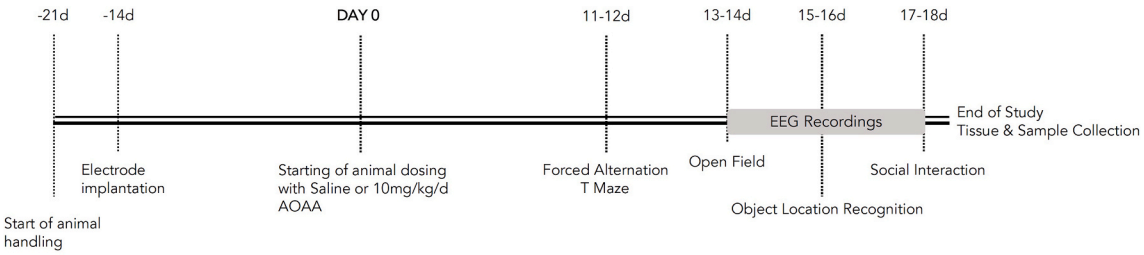

Fig. 14. A visual representation of the experimental design used in the current study.

transition and at the same time period each day. Rats were acclimatized to the corresponding experimental rooms for 20 min prior to commencement of any experimental procedure and behavioral testing. Fig. 14 shows the chronological order of all the described experimental procedures.

The dose of the prototypical CBS inhibitor AOAA [24,25] was based on prior *in vivo* rodent studies [7] and it was also supported by a pilot experiment with WT and Dup(Rno20)Yah (n=6; each genotype) rats of the same age as above. The experiment involved the *ex vivo* treatment of selected brain areas with different AOAA concentrations to evaluate their efficacy in the enzymatic activity of CBS and intracellular ATP production, as described later.

Experimental protocols and purposes of the study were approved and licensed by the Food Safety and Veterinary Affairs Department of the Canton of Fribourg (Reference ID: 2020_05_FR). Animal handling and experiments were performed in accordance with the "Swiss Federal Animal Welfare Act of December 16, 2005". Health state of the rats was assessed daily throughout the study course. Neither treatment-induced harmful side effects nor signs of pain were observed. No premature euthanasia of any animal was conducted.

Western blotting. Following a freeze-thaw cycle, homogenates were sonicated for 5 min (30 s ON; 30 s OFF – 5 cycles) in an ultrasonic water bath (Grant Instruments Ltd., Cambridgeshire, UK) and protein was extracted by centrifugation at 16,000×*g* for 15 min at 4 °C. The BCA assay was employed for protein quantification and samples of whole-cell lysate (20 μg) were separated into 4–12% Bis-Tris protein gels and blotted onto nitrocellulose membranes using our previously published method [26,89]. Membranes were blocked in 5% skimmed milk and probed with the primary antibodies that are listed in Table 2.

Histological and immunohistochemical analysis. Brains were sliced coronally into 40-μm thin sections using a freezing microtome (Leica CM1950, Switzerland) and stored in cryopreserved solution until further use. Free-floating sections were processed similarly as in our previous studies [90,91]. Brain sections were incubated in blocking solution containing 1xTBS, 5% normal goat serum and 0.3% Triton X-100, for 1 h at room temperature. Sections were then incubated in primary antibody solution containing 1xTBS, 1% BSA and 0.3% Triton X-100 overnight at 4 °C. Primary antibodies are listed in Table 2. Following day, the sections were washed twice in TBS and once in Tris-HCl, for 5 min each. Secondary antibodies Goat anti-mouse IgG (H + L) Highly Cross-Adsorbed Secondary Antibody Alexa Fluor Plus 488 (1:1000 dilution), Goat anti-rat IgG (H + L) Highly Cross-Adsorbed Secondary Antibody Alexa Fluor Plus 488 (1:1000 dilution) and Goat anti-rabbit IgG (H + L) Highly Cross-Adsorbed Secondary Antibody Alexa Fluor Plus 568 (1:1000 dilution) were added for 1 h at room temperature. Sections were counterstained with 1 μg/ml DAPI (Merck, MBD0015) for the last 5 min. After final wash, sections were then transfer to microscopy slides and mount with a drop of ProLong™ Gold Antifade Mountant (ThermoFisher Scientific, P36930).

Whole slide scanning. Mounted brain sections were first scanned by a fully automated slide scanner NanoZoomerS60 C13210-01 (Hamamatsu Photonics K. K, Switzerland) with a 20X objective (NA 0.75) and scanning resolution 0.46 μm/pixel and analyzed in NDP.view2 Image viewing software (NanoZoomer, Hamamatsu Photonics K.K, U12388-01). Identical parameters for scanning were applied for parallel-processed sections either in bright-field acquisition or in fluorescent acquisition. Fluorescence images were acquired using the mercury lamp unit using DAPI, FITC, and Cy3 filter cube with excitation filters (387, 485, and 560 nm) and emission filters (410, 504, 582 nm). Specific regions were analyzed using the "free-hand" tool in the NDP.view2 software (Hamamatsu Photonics K. K, Switzerland).

Confocal Microscopy and Image Processing. Leica STELLARIS 8 FALCON inverted laser scanning confocal microscope was used for examination of specific areas of the brain. A 40X water-immersion objective (NA) was used. A DMOD 405 laser was used for DAPI excitation. A pulsed Supercontinuum White Light Laser was used for excitation of Alexa 488 or Alexa568. Proprietary Acousto-Optical Beam Splitter (AOBS) enabled the use of simultaneous independent laser lines. Fluorescence of DAPI was acquired by excitation at Ex 405 nm and recording the emission at Em 415–470 nm, Alexa Fluor™ 488 dye was acquired at Ex 488 nm, Em 498–555 nm and Alexa Fluor™ 568 fluorescence was acquired at Ex 553 nm, Em 570–630 nm. Scanning format used for confocal acquisition was as followed: 1240 x 1240 pixels, scan speed 200 Hz, pinhole diameter 1AU, Z-step interval 0.42-μm. For image

Table 2
Antibodies used for Western blotting (WB) or immunohistochemical (IHC) analysis.

Antibody ID	Dilution Ratio	Clonality	Isotype	Manufacturer	Catalogue No
NeuN (IHC)	1:300	Monoclonal	Mouse IgG	ThermoFisher Scientific	MA5-33103
GFAP (IHC)	1:300	Monoclonal	Mouse IgG	Cell Signaling Technology	#3670
Endothelial cells (IHC)	1:1,000	Monoclonal	Rat IgG	Swant Inc.	288
CBS (IHC)	1:500	Polyclonal	Rabbit IgG	Custom made	[Ref. 96]
CBS (WB)	1:1,000	Monoclonal	Rabbit IgG	Cell Signaling Technology	#14782
3-MST (WB)	1:500	Polyclonal	Rabbit IgG	Abcam	ab154514
CSE (WB)	1:500	Polyclonal	Rabbit IgG	Abcam	ab151769
TST (WB)	1:1,000	Monoclonal	Rabbit IgG	Abcam	ab166625
ETHE1 (WB)	1:1,000	Monoclonal	Rabbit IgG	Abcam	ab174302
SQR (WB)	1:1,000	Polyclonal	Rabbit IgG	Sigma	HPA017079
β-Actin (WB)	1:10,000	Monoclonal	Mouse IgG	Cell Signaling Technology	#3700
PSD95 (D27E11) XP® (WB)	1:1,000	Monoclonal	Rabbit IgG	Cell Signaling Technology	#3450
Synaptophysin (D35E4) (WB)	1:1,000	Monoclonal	Rabbit IgG	Cell Signaling Technology	#5461

reconstruction and morphometric analyses, Imaris 9.7.1® software (Bitplane, AG, Switzerland) was used. For automatic neuron tracing and analysis of neuronal branching, the "Filament Tracer" software package was used. For volume and fluorescence intensity determination "Cell" software package and "Surface" software package of the Imaris software were used as described [91]. The same parameters and algorithm settings were applied for comparison between WT and DS group.

Determination of CBS-mediated H_2S generation in various brain regions *ex vivo*. In a pilot experiment, animals of both genotypes were euthanized by isoflurane overdose, followed by decapitation. The brains were rapidly removed from the skull and dissected into coronal sections of 1 mm. From the sections, we subsequently isolated the prefrontal cortex (PFC), hippocampus (HIP), entorhinal cortex (ETC), and basal forebrain (BF). Two-to-three sections per brain area of interest per rat were placed into a well of a 24-well tissue plate that contained 1 ml of pre-warmed artificial cerebrospinal fluid (aCSF; 120 mM NaCl, 3.5 mM KCl, 1.5 mM $CaCl_2$, 0.4 mM KH_2PO_4, 1 mM $MgCl_2$, HEPES 5 mM) that had been previously supplemented with 4.5 g/l D-glucose, 0.23 mM sodium pyruvate and 4 mg/ml fatty-acid free bovine serum albumin (BSA) and adjusted at the pH of 7.4. Tissue was subsequently treated with 0 or 100 μM AOAA for 1 h at 37 °C before being assayed for CBS activity. At the end of treatment incubation, brain tissue was homogenized by mechanical shearing (~20 strokes) with a Wheaton™ Dounce tissue grinder in pre-cooled radioimmunoprecipitation assay buffer (RIPA buffer) on ice; RIPA buffer was supplemented with 1X Halt™ protease/phosphatase inhibitor cocktail (Thermo Fisher Scientific, Basel, Switzerland). Protein was collected by centrifugation at 10,000×*g* for 10 min at 4 °C. Protein concentration was determined with the BCA assay (Pierce™ BCA Protein Assay Kit by Thermo Fisher Scientific). Protein samples of each experimental condition were then assayed for CBS enzyme activity (H_2S generation), as described [9]. Briefly, the assays were carried out in 96-well flat-bottomed black microplates, using the H_2S-selective fluorescent probe 7-azido-4-methylcoumarin (AzMC; CAS No: 95633-27-5), an Infinite 200 Pro plate reader (Tecan, Männedorf, Switzerland), in a total assay volume of 200 μl. Each well received 50 mM Tris-HCl pH 8.0, 150 μg protein, 5 μM pyridoxal 5′-phosphate hydrate (PLP; AppliChem GmbH, Darmstadt, Germany), 10 μM AzMC, ± 500 μM (5′-adenosyl)-L-methionine (SAM; Cas No: 86867-01-8). The reaction mixture was resuspended 10 times, followed by incubation at room temperature for 10 min in the absence of light. The enzymatic activity was then triggered by dispensing a mixture of 500 μM L-homocysteine (Hcy; CAS No: 6027-13-0) and 2 mM L-cysteine (Cys; AppliChem GmbH) followed by 5 times resuspension. The blanks received buffer in place of homogenate under otherwise identical conditions. The increase in the probe fluorescence ($\lambda_{excitation}$ = 340 nm; $\lambda_{emission}$ = 460 nm) was monitored over 2 h at 37 °C. Enzyme activity was determined from the initial slope of the fluorescence increase over the time. All reagents and supplies required for the assay were acquired from Sigma-Aldrich Chemie GmbH, unless otherwise stated.

Mitochondrial bioenergetics in hippocampal slices; effect of *ex vivo* CBS inhibition. Mitochondrial respiration of coronal hippocampal slices of control and DS rats, in the absence or presence of increasing concentrations of AOAA *ex vivo*, was measured using Seahorse XFe-24 flux analyzer (Agilent Technologies, Santa Clara, California, USA) using XF24 Islet Capture Screen Microplates (Agilent Technologies), as previously described [9]. Following brain tissue isolation and dissection (refer above), hippocampal slides were punched to obtain tissue sections of 1 mm diameter and kept at 37 °C in aCSF. On top of each nylon insert (provided with XF24 Islet Capture Screen – Agilent Seahorse) two hippocampal slices were positioned and fixed with 20 μl of a mixture made of 15 μl of chicken plasma (dissolved in ddH_2O) and 15 μl of thrombin (100 units/ml in a 0.1% (w/v) BSA solution pH 6.5). Using the Seahorse XF Islet Capture Screen Insert Tool (Agilent Technologies), nylon inserts were loaded face down in 16 wells of XF24 Islet Capture Screen Microplate, containing 500 μl of aCSF supplemented with 25 mM glucose, 0.23 mM sodium pyruvate and 4 mg/ml fatty acid-free BSA. From each well 50 μl of assay medium was removed and replaced with an equal volume of AOAA (solubilized in the same medium), yielding 10 μM, 30 μM or 100 μM final concentration (control wells received the same volume of vehicle). Microplates were incubated for 1h in a CO_2-free incubator to allow temperature and pH equilibration. Each measurement cycle consisted in 3 min mix, 3 min wait and 2 min measurement. Basal values of oxygen consumption rate (OCR) were measured, followed by the injection of oligomycin (50 μM; final concentration) to evaluate the ATP generation rate. Data were normalized to protein and per baseline [92].

Implantation of microelectrodes. Anesthesia was induced using 4% isoflurane and was maintained with 1–2% isoflurane in pure O_2 inhalation. The depth of anesthesia was frequently checked and adjusted such that the pedal withdrawal reflex was absent. Animals were placed in a stereotaxic device, a midline incision was made on the scalp, and the periosteum was reflected. Tungsten microelectrodes (FHC Inc. Bowdoin ME, ~400 kΩ) were implanted into the BF (AP -0.8; ML 2.8; DV −8.2) and ETC (AP -0.8; ML 2.8; DV −9) as described [29,93]. The microelectrodes were secured to the skull surface with seven stainless steel screws and dental cement. Six of these screws also served to monitor the EEG, 2 bilateral PFC screws (AP 2.5; ML ± 1), 1 motor cortex (MC) screw (AP -0.8, ML -2), 2 bilateral retrosplenial cortex (RSP) screws (AP -4.4; ML ± 1) and 1 visual cortex (VC) screw (AP -6.5; ML -2). An additional screw over the cerebellum served as a reference. Electrodes and electroencephalogram (EEG) screws were wired to a 10-pin connector.

Electrophysiology and wave form analysis. For electrophysiological analysis, connectors on the head of rats were attached to a miniature wireless head stage (Multichannel Systems, Reutlingen Germany). Signals were acquired at 25 kHz, and the data were stored on a PC for offline analysis. LFPs were downsampled to 1 kHz and were partitioned into 1 s epochs. Epochs containing artifacts were rejected by generating a histogram of peak-to-peak amplitude for each epoch and rejecting epochs during which this value exceeded the median plus1 SD; generally, 10% of the epochs were rejected using this criterion. Artifact-free LFPs were used for all further analyses. Power spectra were calculated as described [29,54] for each epoch by fast Fourier transform. Gamma (γ) power was calculated by taking the mean value of the power spectrum between 30 and 80 Hz. Delta (δ) band, theta (θ) band, and beta (β) band ranges were defined as (1–5 Hz), (6–10 Hz) and (12–30 Hz), respectively [29,93].

Forced alternation T-maze testing. The forced alternation T-maze paradigm builds on an animal's natural preference for the novelty to evaluate working memory [94]. The task was conducted in a wooden T-maze apparatus that consisted of two choice arms (L 60 cm × W 10), branching off at the same point from the start arm and forming a T-shape. The arms were surrounded by a 40-cm high continuous wall. The task comprised two successive trials – the acquisition and the free choice run – with an intertrial interval time of 10 min. Both trials were performed under dim light conditions (15 ± 5 lux). In the acquisition trial, the rat was placed into the start arm, facing the wall and away from the center. The rat was then allowed to explore the apparatus for 5 min with the entry into one of the two choice arms prevented by a guillotine door. During the retention trial, each rat had similarly 5 min to explore the apparatus, with the previously blocking guillotine door now lifted, rendering free access to all choice arms. Animal activity was recorded by the overhead Logitech HD Webcam C270 at all times. At the end of each session, the apparatus was thoroughly cleaned with 70% ethyl alcohol to eliminate residual olfactory cues. Footages were then processed with the tracking/analyzer software ANY-Maze (Stoelting Co., Dublin, Ireland). Each generated track was analyzed for the time spent in the novel and familiar arm of the apparatus within the first minute during the retention trial. The acquired data were further utilized for the calculation of the Success Rate that describes the percent ratio of the time allotted to the novel arm over the total time engaged in both arms. Success Rates exceeding the chance level (50%) indicate spontaneous spatial alternation. The tracks were also analyzed for the latency time to the first

successful entry to the novel arm along with the number of successful entries to the novel arm. Video processing and data handling were performed by an experimenter blinded to the genotype and treatment of the animals.

Open field test (OFT). Relative anxiety levels and general motor function were assessed in the open field test [95]. The testing apparatus consisted of a black-colored square plastic arena (60 × 60 cm) with a metal grid floor and surrounded by a continuous wall 40-cm-high wall. Light intensity of 15 ± 5 lux was reaching the apparatus. Each rat was gently placed into the center of the arena and allowed to freely explore the apparatus for 10 min, with the experimenter out of the animal's sight. White noise at 60 dB was produced over the open-field course to cover any background noise and the activity of the animal in the arena was video-recorded with the HD ultra-wide Genius WideCam F100 mounted above the arena. At the end of each trial, any fecal deposits were removed, and the apparatus was thoroughly cleaned with 70% ethanol to eliminate any residual olfactory cues. Footages were subsequently processed with the automated tracking/analyzer software ANY-maze. Within the software, the testing arena was divided into 25 squares (12 × 12 cm each). The four squares located in the central area covering an area of 24 × 24 cm were designated as the central zone, and the four squares located at each corner defined the thigmotactic corners. Each generated track represented the total distance traveled per minute and analyzed for the percentage of time spent in the corners to quantify the percentage of thigmotaxis per minute. Each generated track was additionally analyzed for the total time spent and number of entries in the central zone along with the mean velocity over the course session. Processing of all video recordings was carried out by an experimenter blinded to the genotype and treatment of the animals.

Object-location recognition test. The object-location paradigm builds on an animal's natural preference for the novelty to evaluate the spatial components of the episodic memory [94]. It comprised two successive trials – the acquisition and the retention trial – with an inter-trial interval time of 10 min. The acquisition trial commenced 48h following the OFT and involved placing the rat in the center of the familiar open-field arena that at the time contained two identical objects placed along a straight line 10-cm away from the nearest wall. Each rat was allowed to freely explore the objects for 3 min. Ten minutes later, a retention trial followed, during which each rat was assigned to reexplore the familiar arena that at that time contained one object at the same location as in the acquisition trial and the second object positioned diagonally opposite to the first one (novel location). The retention trial lasted for 3 min and aimed to assess the animal's place recognition memory. Over both trials, light and noise conditions remained identical to the ones during the OFT. We recorded the activity of each rat over sample and choice sessions using the overhead Genius WideCam F100. At the end of each session, the apparatus and the objects were thoroughly cleaned with 70% ethyl alcohol to eliminate any residual olfactory cues. Footages were subsequently processed with the automated tracking/analyzer software ANY-maze to quantify the exploration time allotted in each object during acquisition and retention trials. A rat is considered to explore an object when its nose is within a distance of 2 cm from the object. Acquired data were then processed for the calculation of the Recognition Index that describes the percent ratio of the time spent in the object in the familiar or novel location over the total time spent in object exploration during the retention trial. A Recognition Index for the novel location exceeding the chance level (50%) indicated the formation of spontaneous place recognition memory. We also recorded and compared the total exploration time allotted to the objects during the acquisition trial, along with the velocity and total path length of each animal in the retention trial to ascertain that no lack of motivation or emotional defects had interfered with the task acquisition and memory testing. Processing of all video recordings was carried out by an experimenter blinded to the genotype and treatment of the animals.

Social interaction test. Social interaction paradigm, adapted by Aqrabawi [95], was employed for assessing the social recognition memory. The latter describes the ability to learn and distinguish between familiar and novel conspecifics, a key component of social behavior function. The task was carried out in the open-field apparatus under identical light and noise conditions like the ones during OFT. It comprised an acquisition and a retention trial with an inter-trial interval time of 10 min. During acquisition, the arena was enriched with two identical transparent cylindrical cages for sociability, positioned opposite 10-cm away for the nearest walls; one cage contained a male juvenile rat (3 weeks old) while the second cage was left empty. Each rat was allowed to freely explore the arena for 5 min. After 10 min, rats underwent a retention trial of 5 min, during which the first, now-familiar, animal was placed in the previously empty cage and a second juvenile male rat – unfamiliar with the test subject – was added to the cylindrical cage that was previously occupied. In both sociability and social novelty preference phases, we recorded the activity of the rats using the overhead Genius WideCam F100. At the end of each session, the apparatus and the cages were thoroughly cleaned with 70% ethyl alcohol to eliminate any residual olfactory cues. Footages were subsequently processed with the automated tracking/analyzer software ANY-maze for quantifying the interaction time with either cage to determine the animal sociability. Direct interaction with the testing subject's nose in contact with each cage was scored in our analysis. Acquired data were further processed for the calculation of the Preference Index that describes the percent ratio of the time allotted to the novel or familiar social target over the total time engaged in interacting with either cage during the retention trial. Preference Index exceeding the chance level (50%) indicated a preference for social novelty. Behavioral scoring and data analysis were performed by an experimenter blind to the genotype and assigned treatment groups of the rats.

Collection and processing of blood and brain tissue. Upon completion of the neurobehavioral assessment, rats were terminally anesthetized by isoflurane inhalation and euthanized by decapitation. Trunk blood was collected into micro sample tubes with heparin (Sarstedt, Sevelen, Switzerland) and processed for VetScan® analysis (Abaxis Europe GmbH, Griesheim, Germany). Brains were rapidly removed from the skull and dissected into coronal sections of 1 mm on ice. From the sections, we subsequently isolated the prefrontal cortex (PFC), hippocampus (HIP), entorhinal cortex (ETC), and basal forebrain (BF) that were homogenized by mechanical shearing with a Wheaton™ Dounce tissue grinder in pre-cooled N-PER® Neuronal Protein Extraction Reagent (Thermo Fisher Scientific) supplemented with protease/phosphatase inhibitor cocktail (1x). Homogenates were stored at −80 °C

Table 3
Experimental group sizes used in the current study.

Genotype	Behavioral & Cognitive Assessment	Electrophysiology	Western Blotting	Histology	Vetscan	H_2S generation	ATP production
In vivo AOAA treatment/*in vivo* or *ex vivo* analysis							
WT/Saline	11	9	5	5	8		
WT/AOAA	11	9	5	5	8		
Dup(Rno20)Yah/Saline	11	9	5	5	8		
Dup(Rno20)Yah/AOAA	11	9	5	5	8		
Tissue collection followed by *in vitro* AOAA treatment and analysis							
WT						6	6
Dup(Rno20)Yah						6	6

until processed for immunoblotting studies. Alternatively, collected brains were immersion-fixed in 4% paraformaldehyde for 48h each at 4 °C and cryoprotected into 30% sucrose in PBS solution. Brain tissue was then embedded on the specimen stage using Tissue-Tek® O.C.T. compound, snap-frozen with Ice-It™ Freezing Spray, and sectioned in the coronal plane at 40 μm on a Leica cryostat (Leica Microsystems Ltd, Buckinghamshire, UK). Sections were sampled in accordance with the stereological rules, with the first one retained randomly and every 12th section afterwards that rendered 7–12 coronal sections throughout the cortex and limbic system per animal for quantitative analysis. Sections were preserved in 30% ethylene glycol and 25% glycerol in 0.1 M phosphate buffer (pH 7.4) at −20 °C until processed for immunohistochemical assessments.

Statistical analysis. All the results were expressed as mean ± standard error (SEM) of 11 animals for the behavioral/cognitive studies and of 5–9 animals for immunoassays and functional analysis (Table 3). Differences among means were considered significant when $p \leq 0.05$. The assumption of data normality examined with either the Shapiro-Wilk test or D'Agostino & Pearson test. Data were processed with two-way or three-way ANOVA, followed by *post-hoc* Bonferroni's multiple comparison tests, except for histological data. The latter was analyzed with (LUCIA's input needed here). Statistical calculations were performed in GraphPad Prism 9 (GraphPad Software Inc., San Diego, USA).

Author contributions

Theodora Panagaki: contributed to experimental design; performed experiments and collected data; contributed to paper writing; Laura Lozano-Montes: contributed to experimental design; Performed experiments and collected data; contributed to paper writing; Lucia Janickova: performed experiments and collected data; performed data analysis; contributed to paper writing; Karim Zuhra: performed experiments and collected data; performed data analysis; contributed to paper writing; Marcell P. Szabo: performed experiments and collected data; performed data analysis; contributed to paper writing; Tomas Majtan: performed experiments; Gregor Rainer: contributed to experimental design; provided specific experimental tools; contributed to paper writing; Damien Marechal: performed experiments and provided specific experimental tools; Yann Herault: obtained funding for the work; contributed to experimental design; provided specific experimental tools; contributed to paper writing; Csaba Szabo: obtained funding for the work, had primary role in the formulation of the working hypothesis and the experimental design of the study, contributed to specific experimental design and data analysis; contributed to paper writing; wrote the discussion of the paper.

Declaration of competing interest

None.

Acknowledgements

The technical assistance of Mr. Olivier Bremer is appreciated. This work was supported by grants from the Lejeune Foundation (Paris) to C. S. and Y.H and by the Bettencourt-Schueller Foundation to Y.H.

References

[1] A. Ruparelia, F. Wiseman, O. Sheppard, V.L.J. Tybulewicz, E.M.C. Fisher, Down syndrome and the molecular pathogenesis resulting from trisomy of human chromosome 21, J. Biomed. Res. 24 (2010) 87–99.
[2] M.S. Rafii, A.M. Kleschevnikov, M. Sawa, W.C. Mobley, Down syndrome, Handb. Clin. Neurol. 167 (2019) 321–336.
[3] L. Pecze, E.B. Randi, C. Szabo, Meta-analysis of metabolites involved in bioenergetic pathways reveals a pseudohypoxic state in Down syndrome, Mol. Med. 26 (2020) 102.
[4] L. Pecze, C. Szabo, Meta-analysis of gene expression patterns in Down syndrome highlights significant alterations in mitochondrial and bioenergetic pathways, Mitochondrion 57 (2021) 163–172.
[5] P.P. Kamoun, Mental retardation in Down syndrome: two ways to treat, Med. Hypotheses 131 (2019) 109289.
[6] C. Szabo, The re-emerging pathophysiological role of the cystathionine-β-synthase - hydrogen sulfide system in Down syndrome, FEBS J. 287 (2020) 3150–3160.
[7] K. Zuhra, F. Augsburger, T. Majtan, C. Szabo, Cystathionine-β-synthase: molecular regulation and pharmacological inhibition, Biomolecules 10 (2020) 697.
[8] T. Panagaki, E.B. Randi, F. Augsburger, C. Szabo, Overproduction of H_2S, generated by CBS, inhibits mitochondrial Complex IV and suppresses oxidative phosphorylation in Down syndrome, Proc. Natl. Acad. Sci. U.S.A. 116 (2019) 18769–18771.
[9] K. Zuhra, T. Panagaki, E.B. Randi, F. Augsburger, M. Blondel, G. Friocourt, Y. Herault, C. Szabo, Mechanism of cystathionine-β-synthase inhibition by disulfiram: the role of bis(N,N-diethyldithiocarbamate)-copper(II), Biochem. Pharmacol. 182 (2020) 114267.
[10] D. Marechal, V. Brault, A. Leon, D. Martin, P. Lopes Pereira, N. Loaëc, M.C. Birling, G. Friocourt, M. Blondel, Y. Herault, CBS overdosage is necessary and sufficient to induce cognitive phenotypes in mouse models of Down syndrome and interacts genetically with Dyrk1a, Hum. Mol. Genet. 28 (2019) 1561–1577.
[11] Y. Herault, J.M. Delabar, E.M.C. Fisher, V.L.J. Tybulewicz, E. Yu, V. Brault, Rodent models in Down syndrome research: impact and future opportunities, Dis. Model Mech. 10 (2017) 1165–1186.
[12] M.D.M. Muñiz Moreno, V. Brault, M.C. Birling, G. Pavlovic, Y. Herault, Modeling Down syndrome in animals from the early stage to the 4.0 models and next, Prog. Brain Res. 251 (2020) 91–143.
[13] M.C. Birling, Y. Herault, G. Pavlovic, Modeling human disease in rodents by CRISPR/Cas9 genome editing, Mamm. Genome 28 (2017) 291–301.
[14] M.S. Cheon, M. Bajo, S.H. Kim, J.O. Claudio, A.K. Stewart, D. Patterson, W. D. Kruger, H. Kondoh, G. Lubec, Protein levels of genes encoded on chromosome 21 in fetal Down syndrome brain: challenging the gene dosage effect hypothesis (Part II), Amino Acids 24 (2003) 119–125.
[15] J.H. Shin, R. Weitzdoerfer, M. Fountoulakis, G. Lubec, Expression of cystathionine beta-synthase, pyridoxal kinase, and ES1 protein homolog (mitochondrial precursor) in fetal Down syndrome brain, Neurochem. Int. 45 (2004) 73–79, 2004.
[16] A. Ichinohe, T. Kanaumi, S. Takashima, Y. Enokido, Y. Nagai, H. Kimura, Cystathionine beta-synthase is enriched in the brains of Down's patients, Biochem. Biophys. Res. Commun. 338 (2005) 1547–1550.
[17] T. Kanaumi, A. Ichinohe, H. Kimura, H. Iwasaki, S. Hirose, S. Takashima, Development and aging expression of cystathionine-beta synthase in the temporal lobe and cerebellum of Down syndrome patients, Neuroembryol. Aging 4 (2006) 202–207.
[18] E. Dossi, F. Vasile, N. Rouach N, Human astrocytes in the diseased brain, Brain Res. Bull. 136 (2018) 139–156.
[19] C. Reilly, Autism spectrum disorders in Down syndrome: a review, Res. Autism Spectrum Dis. 3 (2009) 829–839.
[20] C.C. Garner, D.Z. Wetmore, Synaptic pathology of Down syndrome, Adv. Exp. Med. Biol. 970 (2012) 451–468.
[21] M.C. Belardinelli, A. Chabli, B. Chadefaux-Vekemans, P. Kamoun, Urinary sulfur compounds in Down syndrome, Clin. Chem. 47 (2001) 1500–1501.
[22] P. Kamoun, M.C. Belardinelli, A. Chabli, K. Lallouchi, B. Chadefaux-Vekemans, Endogenous hydrogen sulfide overproduction in Down syndrome, Am. J. Med. Genet. A. 116A (2003) 310–311.
[23] E. Abdel-Salam, I. Abdel-Meguid, S. Korraa, Assessment of immune function in Down syndrome patients, Egypt. J. Med. Hum. Genet. 14 (2013) 307–310.
[24] A. Asimakopoulou, P. Panopoulos, C.T. Chasapis, C. Coletta, Z. Zhou, G. Cirino, A. Giannis, C. Szabo, G.A. Spyroulias, A. Papapetropoulos, Selectivity of commonly used pharmacological inhibitors for cystathionine β synthase (CBS) and cystathionine γ lyase (CSE), Br. J. Pharmacol. 169 (2013) 922–932.
[25] C. Szabo, A. Papapetropoulos, International union of basic and clinical pharmacology. CII: pharmacological modulation of H_2S levels: H_2S donors and H_2S biosynthesis inhibitors, Pharmacol. Rev. 69 (2017) 497–564.
[26] T. Panagaki, E.B. Randi, C. Szabo, Role of 3-mercaptopyruvate sulfurtransferase in the regulation of proliferation and cellular bioenergetics in human Down syndrome fibroblasts, Biomolecules 10 (2020) 653.
[27] D.R. Linden, J. Furne, G.J. Stoltz, M.S. Abdel-Rehim, M.D. Levitt, H. Szurszewski, Sulphide quinone reductase contributes to hydrogen sulphide metabolism in murine peripheral tissues but not in the CNS, Br. J. Pharmacol. 165 (2012) 2178–2190.
[28] S.S. Nandi, P.K. Mishra, H_2S and homocysteine control a novel feedback regulation of cystathionine beta synthase and cystathionine gamma lyase in cardiomyocytes, Sci. Rep. 7 (2017) 3639.
[29] D. Wu, J. Li, Q. Zhang, W. Tian, P. Zhong, Z. Liu, H. Wang, H. Wang, A. Ji, Y. Li, Exogenous hydrogen sulfide regulates the growth of human thyroid carcinoma cells, Oxid. Med. Cell. Longev. (2019) 6927298, 2019.
[30] E.A. Ostrakhovitch, S. Akakura, R. Sanokawa-Akakura, S. Tabibzadeh, 3-Mercaptopyruvate sulfurtransferase disruption in dermal fibroblasts facilitates adipogenic trans-differentiation, Exp. Cell Res. 385 (2019) 111683.
[31] K. Ascenção, N. Dilek, F. Augsburger, T. Panagaki, K. Zuhra, C. Szabo, Pharmacological induction of mesenchymal-epithelial transition via inhibition of H_2S biosynthesis and consequent suppression of ACLY activity in colon cancer cells, Pharmacol. Res. 165 (2021) 105393.
[32] M. Ersoy, V. Tiranti, M. Zeviani, Ethylmalonic encephalopathy: clinical course and therapy response in an uncommon mild case with a severe ETHE1 mutation, Mol. Genet. Metab. Rep. 25 (2020) 100641.

[33] T. Majtan, A.L. Pey, P. Gimenez-Mascarell, L.A. Martínez-Cruz, C. Szabo, V. Kožich, J.P. Kraus, Potential pharmacological chaperones for cystathionine beta-synthase-deficient homocystinuria, Handb. Exp. Pharmacol. 245 (2018) 345–383.

[34] J. Nair, A.L. Klaassen, J. Arato, A.L. Vyssotski, M. Harvey, G. Rainer, Basal forebrain contributes to default mode network regulation, Proc. Natl. Acad. Sci. U. S.A. 115 (2018) 1352–1357.

[35] M. Ruiz-Mejias, M. Martinez de Lagran, M. Mattia, P. Castano-Prat, L. Perez-Mendez, L. Ciria-Suarez, T. Gener, B. Sancristobal, J. García-Ojalvo, A. Gruart, J. M. Delgado-García, M.V. Sanchez-Vives, M. Dierssen, Overexpression of Dyrk1A, a Down syndrome candidate, decreases excitability and impairs gamma oscillations in the prefrontal cortex, J. Neurosci. 36 (2016) 3648–3659.

[36] M. Ruiz-Mejias, Outer brain oscillations in Down syndrome, Front. Syst. Neurosci. 13 (2019) 17.

[37] J. Zorrilla de San Martin, C. Donato, J. Peixoto, A. Aguirre, V. Choudhary, A.M. De Stasi, J. Lourenço, M.C. Potier, A. Bacci, Alterations of specific cortical GABAergic circuits underlie abnormal network activity in a mouse model of Down syndrome, Elife 9 (2020), e58731.

[38] N. Byron, A. Semenova, S. Sakata, Mutual interactions between brain states and Alzheimer's disease pathology: a focus on gamma and slow oscillations, Biology 10 (2021) 707.

[39] A.G. Isla, H. Balleza-Tapia, A. Fisahn, Efficacy of preclinical pharmacological interventions against alterations of neuronal network oscillations in Alzheimer's disease: a systematic review, Exp. Neurol. 343 (2021) 113743.

[40] R.K. Powers, R. Culp-Hill, M.P. Ludwig, K.P. Smith, K.A. Waugh, R. Minter, K. D. Tuttle, H.C. Lewis, A.L. Rachubinski, R.E. Granrath, M. Carmona-Iragui, R. B. Wilkerson, D.E. Kahn, M. Joshi, A. Lleó, R. Blesa, J. Fortea, A. D'Alessandro, J. C. Costello, K.D. Sullivan, J.M. Espinosa, Trisomy 21 activates the kynurenine pathway via increased dosage of interferon receptors, Nat. Commun. 10 (2019) 4766.

[41] I.S. Muskens, S. Li, T. Jackson, N. Elliot, H.M. Hansen, S.S. Myint, P. Pandey, J. M. Schraw, R. Roy, J. Anguiano, K. Goudevenou, K.D. Siegmund, P.J. Lupo, M.F.T. R. de Bruijn, K.M. Walsh, P. Vyas, X. Ma, A. Roy, I. Roberts, J.L. Wiemels, A.J. de Smith, The genome-wide impact of trisomy 21 on DNA methylation and its implications for hematopoiesis, Nat. Commun. 12 (2021) 821.

[42] E.S. Roberts, R.S. Thomas, D.C. Dorman, Gene expression changes following acute hydrogen sulfide (H_2S)-induced nasal respiratory epithelial injury, Toxicol. Pathol. 36 (2008) 560–567.

[43] E.C. Rios, B. Szczesny, F.G. Soriano, G. Olah, C. Szabo, Hydrogen sulfide attenuates cytokine production through the modulation of chromatin remodeling, Int. J. Mol. Med. 35 (2015) 1741–1746.

[44] C.M. Phillips, J.R. Zatarain, M.E. Nicholls, C. Porter, S.G. Widen, K. Thanki, P. Johnson, M.U. Jawad, M.P. Moyer, J.W. Randall, J.L. Hellmich, M. Maskey, S. Qiu, T.G. Wood, N. Druzhyna, B. Szczesny, K. Módis, C. Szabo, C. Chao, M. R. Hellmich, Upregulation of cystathionine-β-synthase in colonic epithelia reprograms metabolism and promotes carcinogenesis, Cancer Res. 77 (2017) 5741–5754.

[45] K. Módis, V.S. Ramanujam, A.A. Govar, E. Lopez, K.E. Anderson, R. Wang, C. Szabo, Cystathionine-γ-lyase (CSE) deficiency increases erythropoiesis and promotes mitochondrial electron transport via the upregulation of coproporphyrinogen III oxidase and consequent stimulation of heme biosynthesis, Biochem. Pharmacol. 169 (2019) 113604.

[46] S.I. Bibli, J. Hu, F. Sigala, I. Wittig, J. Heidler, S. Zukunft, D.I. Tsilimigras, V. Randriamboavonjy, J. Wittig, B. Kojonazarov, C. Schürmann, M. Siragusa, D. Siuda, B. Luck, R. Abdel Malik, K.A. Filis, G. Zografos, C. Chen, D.W. Wang, J. Pfeilschifter, R.P. Brandes, C. Szabo, A. Papapetropoulos, I. Fleming, Cystathionine γ lyase sulfhydrates the RNA binding protein human antigen R to preserve endothelial cell gunction and delay atherogenesis, Circulation 139 (2019) 101–114.

[47] R. Guan, J. Wang, Z. Cai, Z. Li, L. Wang, Y. Li, J. Xu, D. Li, H. Yao, W. Liu, B. Deng, W. Lu, Hydrogen sulfide attenuates cigarette smoke-induced airway remodeling by upregulating SIRT1 signaling pathway, Redox Biol. 28 (2020) 101356.

[48] C. Chen, P. Jiang, H. Xue, S.E. Peterson, H.T. Tran, A.E. McCann, M.M. Parast, S. Li, D.E. Pleasure, L.C. Laurent, J.F. Loring, Y. Liu, W. Deng, Role of astroglia in Down's syndrome revealed by patient-derived human-induced pluripotent stem cells, Nat. Commun. 5 (2014) 4430.

[49] G.O. Mizuno, Y. Wang, G. Shi, Y. Wang, J. Sun, S. Papadopoulos, G.J. Broussard, E. K. Unger, W. Deng, J. Weick, A. Bhattacharyya, C.Y. Chen, G. Yu, L.L. Looger, L. Tian, Aberrant calcium signaling in astrocytes inhibits neuronal excitability in a human Down syndrome stem cell model, Cell Rep. 24 (2018) 355–365.

[50] B.H.S. Araujo, C. Kaid, J.S. De Souza, S. Gomes da Silva, E. Goulart, L.C.J. Caires, C. M. Musso, L.B. Torres, A. Ferrasa, R. Herai, M. Zatz, O.K. Okamoto, E. A. Cavalheiro, Down syndrome iPSC-derived astrocytes impair neuronal synaptogenesis and the mTOR pathway in vitro, Mol. Neurobiol. 55 (2018) 5962–5975.

[51] V.L. Savchenko, I.R. Nikonenko, G.G. Skibo, J.A. McKanna, Distribution of microglia and astrocytes in different regions of the normal adult rat brain, Neurophysiology 29 (1997) 343–351.

[52] M.M. Sanchez, S. Moghadam, P. Naik, K.J. Martin, A. Salehi, Hippocampal network alterations in Alzheimer's disease and Down syndrome: from structure to therapy, J. Alzheimers Dis. 26S (2011) 29–47.

[53] M.R. Bronzuoli, R. Facchinetti, L. Steardo, C. Scuderi, Astrocyte: an innovative approach for Alzheimer's Disease therapy, Curr. Pharmaceut. Des. 23 (2017) 4979–4989.

[54] A. Freeburn, R.G.K. Munn, Signalling pathways contributing to learning and memory deficits in the Ts65Dn mouse model of Down syndrome, Neuronal. Signal. 5 (2021), NS20200011.

[55] T. Kitamura, C.J. Macdonald, S. Tonegawa, Entorhinal-hippocampal neuronal circuits bridge temporally discontiguous events, Learn. Mem. 22 (2015) 438–443.

[56] A.Ö. Sungur, R.K.W. Schwarting, M. Wöhr, Behavioral phenotypes and neurobiological mechanisms in the Shank1 mouse model for autism spectrum disorder: a translational perspective, Behav. Brain Res. 352 (2018) 46–61.

[57] H. Arakawa, From multisensory assessment to functional interpretation of social behavioral phenotype in transgenic mouse models for autism spectrum disorders, Front. Psychiatr. 11 (2020) 592408.

[58] F. Filice, L. Janickova, T. Henzi, A. Bilella, B. Schwaller, The Parvalbumin Hypothesis of autism spectrum disorder, Front. Cell. Neurosci. 14 (2020) 577525.

[59] M. Borgogno, A. Savardi, J. Manigrasso, A. Turci, C. Portioli, G. Ottonello, S. M. Bertozzi, A. Armirotti, A. Contestabile, L. Cancedda, M. De Vivo, Indeed, design, synthesis, in vitro and in vivo characterization of selective NKCC1 inhibitors for the treatment of core symptoms in Down syndrome, J. Med. Chem. 64 (2021) 10203–10229.

[60] V. Brault, T.L. Nguyen, J. Flores-Gutiérrez, G. Iacono, M.C. Birling, V. Lalanne, H. Meziane, A. Manousopoulou, G. Pavlovic, L. Lindner, M. Selloum, T. Sorg, E. Yu, S.D. Garbis, Y. Hérault, Dyrk1a gene dosage in glutamatergic neurons has key effects in cognitive deficits observed in mouse models of MRD7 and Down syndrome, PLoS Genet. 17 (2021), e1009777.

[61] M.L. Arbones, A. Thomazeau, A. Nakano-Kobayashi, M. Hagiwara, J.M. Delabar, DYRK1A and cognition: a lifelong relationship, Pharmacol. Ther. 194 (2019) 199–221.

[62] O.H. Kim, H.J. Cho, E. Han, T.I. Hong, K. Ariyasiri, J.H. Choi, K.S. Hwang, Y. M. Jeong, S.Y. Yang, K. Yu, D.S. Park, H.W. Oh, E.E. Davis, C.E. Schwartz, J.S. Lee, H.G. Kim, C.H. Kim, Zebrafish knockout of Down syndrome gene, DYRK1A, shows social impairments relevant to autism, Mol. Autism. 8 (2017) 50.

[63] F.C. Gomes, M.F. Mattos, E.M. Goloni-Bertollo, É.C. Pavarino, Alzheimer's disease in the Down syndrome: an overview of genetics and molecular aspects, Neurol. India 69 (2021) 32–41.

[64] D. Gabuzda, J. Busciglio, L.B. Chen, P. Matsudaira, B.A. Yankner, Inhibition of energy metabolism alters the processing of amyloid precursor protein and induces a potentially amyloidogenic derivative, J. Biol. Chem. 269 (1994) 13623–13628.

[65] G. Monzio Compagnoni, A. Di Fonzo, S. Corti, G.P. Comi, N. Bresolin, E. Masliah, The role of mitochondria in neurodegenerative diseases: the lesson from Alzheimer's disease and Parkinson's disease, Mol. Neurobiol. 57 (2020) 2959–2980.

[66] M.T. Lin, M.F. Beal, Mitochondrial dysfunction and oxidative stress in neurodegenerative diseases, Nature 443 (2006) 787–795.

[67] F. Di Domenico, E. Barone, M. Perluigi, D.A. Butterfield, The Triangle of Death in Alzheimer's Disease brain: the aberrant cross-talk among energy metabolism, Mammalian target of Rapamycin Signaling, and protein homeostasis revealed by redox proteomics, Antioxidants Redox Signal. 26 (2017) 364–387.

[68] T. Panagaki, E.B. Randi, C. Szabo, Role of hydrogen sulfide and 3-mercaptopyruvate sulfurtransferase in the regulation of the endoplasmic reticulum stress response in hepatocytes, Biomolecules 10 (2020) 1692.

[69] G. Monzio Compagnoni, A. Di Fonzo, S. Corti, G.P. Comi, N. Bresolin, E. Masliah, The role of mitochondria in neurodegenerative diseases: the lesson from Alzheimer's Disease and Parkinson's Disease, Mol. Neurobiol. 57 (2020) 2959–2980.

[70] H. Murali Mahadevan, A. Hashemiaghdam, G. Ashrafi, A.B. Harbauer, Mitochondria in neuronal health: from energy metabolism to Parkinson's disease, Adv. Biol. (Weinh). 5 (2021), e2100663.

[71] M.P. Szabo, S. Mishra, A. Knupp, J.E. Young, The role of Alzheimer's disease risk genes in endolysosomal pathways, Neurobiol. Dis. 62 (2021) 105576.

[72] C. Sharma, S. Kim, Y. Nam, U.J. Jung, S.R. Kim, Mitochondrial dysfunction as a driver of cognitive impairment in Alzheimer's Disease, Int. J. Mol. Sci. 22 (2021) 4850.

[73] N. Druzhyna, B. Szczesny, G. Olah, K. Módis, A. Asimakopoulou, A. Pavlidou, P. Szoleczky, D. Gerö, K. Yanagi, G. Törö, I. López-García, V. Myrianthopoulos, E. Mikros, J.R. Zatarain, C. Chao, A. Papapetropoulos, M.R. Hellmich, C. Szabo, Screening of a composite library of clinically used drugs and well-characterized pharmacological compounds for cystathionine β-synthase inhibition identifies benserazide as a drug potentially suitable for repurposing for the experimental therapy of colon cancer, Pharmacol. Res. 113 (2016) 18–37.

[74] J.D. Wood, S.J. Peesker, The role of GABA metabolism in the convulsant and anticonvulsant actions of aminooxyacetic acid, J. Neurochem. 20 (1973) 379–387.

[75] J.D. Wood, S.J. Peesker, A dual mechanism for the anticonvulsant action of aminooxyacetic acid, Can. J. Physiol. Pharmacol. 54 (1976) 534–540.

[76] G. Tunnicliff, T.T. Ngo, J.M. Rojo-Ortega, A. Barbeau, The inhibition by substrate analogues of gamma-aminobutyrate aminotransferase from mitochondria of different subcellular fractions of rat brain, Can. J. Biochem. 55 (1977) 479–484.

[77] W. Löscher, A comparative study of the pharmacology of inhibitors of GABA-metabolism, Naunyn-Schmiedeberg's Arch. Pharmacol. 315 (1980) 119–128.

[78] K. Gale, M.J. Iadarola, Seizure protection and increased nerve-terminal GABA: delayed effects of GABA transaminase inhibition, Science 208 (1980) 288–291.

[79] E. Carmona, C. Gomes, G. Trolin, On the importance of GABA-ergic neurons for the AOAA induced accumulation of GABA in the rat brain, Naunyn-Schmiedeberg's Arch. Pharmacol. 313 (1980) 221–224.

[80] C. Gomes, G. Trolin, GABA turnover in mouse brain: agreement between the rate of GABA accumulation after aminooxyacetic acid and the rate of disappearance after 3-mercaptopropionic acid, J. Neural. Transm. 54 (1982) 265–274.

[81] A.J. Davison, Aminooxyacetic acid provides transient protection against seizures induced by hyperbaric oxygen, Brain Res. 276 (1983) 384–387.

[82] S.R. Pagliusi, C. Gomes, J.R. Leite, G. Trolin, Aminooxyacetic acid induced accumulation of GABA in the rat brain. Interaction with GABA receptors and

distribution in compartments, Naunyn-Schmiedeberg's Arch. Pharmacol. 322 (1983) 210–215.
[83] A.R. Green, A. Metz, M.C. Minchin, N.D. Vincent, Inhibition of the rate of GABA synthesis in regions of rat brain following a convulsion, Br. J. Pharmacol. 92 (1987) 5–11.
[84] A. Contestabile, S. Magara, L. Cancedda, The GABAergic hypothesis for cognitive disabilities in Down syndrome, Front. Cell. Neurosci. 11 (2017) 54.
[85] J. Zorrilla de San Martin, J.M. Delabar, A. Bacci, M.C. Potier, GABAergic over-inhibition, a promising hypothesis for cognitive deficits in Down syndrome, Free Radic. Biol. Med. 114 (2018) 33–39.
[86] N. Rueda, J. Flórez, M. Dierssen, C. Martínez-Cué, Translational validity and implications of pharmacotherapies in preclinical models of Down syndrome, Prog. Brain Res. 251 (2020) 245–268.
[87] S. Coghlan, J. Horder, B. Inkster, M.A. Mendez, D.G. Murphy, D.J. Nutt, GABA system dysfunction in autism and related disorders: from synapse to symptoms, Neurosci. Biobehav. Rev. 36 (2012) 2044–2055.
[88] W. Zhang, B.R. Xiong, L.Q. Zhang, X. Huang, X. Yuan, Y.K. Tian, X.B. Tian, The role of the GABAergic system in diseases of the central nervous system, Neuroscience 470 (2021) 88–99.
[89] T. Panagaki, S. Gengler, C. Hölscher, The novel DA-CH3 dual incretin restores endoplasmic reticulum stress and autophagy impairments to attenuate Alzheimer-like pathology and cognitive decrements in the APPSWE/PS1ΔE9 mouse model, J. Alzheimers Dis. 66 (2018) 195–218.
[90] L. Janickova, B. Schwaller, Parvalbumin-deficiency accelerates the age-dependent ROS production in Pvalb neurons in vivo: link to neurodevelopmental disorders, Front. Cell. Neurosci. 14 (2020) 571216.
[91] L. Janickova, K.F. Rechberger, L. Wey, B. Schwaller, Absence of parvalbumin increases mitochondria volume and branching of dendrites in inhibitory Pvalb neurons in vivo: a point of convergence of autism spectrum disorder (ASD) risk gene phenotypes, Mol. Autism. 11 (2020) 47.
[92] R.A. Schuh, P. Clerc, H. Hwang, Z. Mehrabian, K. Bittman, H. Chen, B.M. Polster, Adaptation of microplate-based respirometry for hippocampal slices and analysis of respiratory capacity, J. Neurosci. Res. 89 (2011) 1979–1988.
[93] L. Lozano-Montes, M. Dimanico, R. Mazloum, W. Li, J. Nair, M. Kintscher, R. Schneggenburger, M. Harvey, G. Rainer, Optogenetic stimulation of basal forebrain parvalbumin neurons activates the default mode network and associated behaviors, Cell Rep. 33 (2020) 108359.
[94] R. Bevins, J. Besheer, Object recognition in rats and mice: a one-trial non-matching-to-sample learning task to study 'recognition memory, Nat. Protoc. 1 (2006) 1306–1311.
[95] A.J. Aqrabawi, C.J. Browne, Z. Dargaei, D. Garand, C.S. Khademullah, M. A. Woodin, J.C. Kim, Top-down modulation of olfactory-guided behaviours by the anterior olfactory nucleus pars medialis and ventral hippocampus, Nat. Commun. 7 (2016) 13721.
[96] T. Majtan, L.R. Singh, L. Wang, W.D. Kruger, J.P. Kraus, Active cystathionine beta-synthase can be expressed in heme-free systems in the presence of metal-substituted porphyrins or a chemical chaperone, J. Biol. Chem. 283 (2008) 34588–34595.